TAMPEREEN TEKNILLINEN YLIOPISTO
TAMPERE UNIVERSITY OF TECHNOLOGY

OLLI PARTANEN

OPTIMIZATION OF SOLID SOLUTION STRENGTHENED FERRITIC DUCTILE IRON PRODUCTION BY THERMAL ANALYSIS AND SOLIDIFICATION SIMULATION

Master of Science thesis

Examiner: Doc. Juhani Orkas and Assoc. Prof. Pasi Peura
Examiner and topic approved by the Faculty Council of the Faculty of Engineering Sciences
on 9th March 2016

ABSTRACT

OLLI PARTANEN: Optimization of solid solution strengthened ferritic ductile iron production by thermal analysis and solidification simulation
Tampere University of Technology
Master of Science thesis, 53 pages
April 2016
Master's Degree Programme in Materials Engineering
Major: Metallic Materials
Examiner: Doc. Juhani Orkas and Assoc. Prof. Pasi Peura
Keywords: GJS 600–10, ductile iron, solid solution strengthening, cooling curve analysis, solidification simulation

The newest EN 1563 standard about ductile iron castings was published in 2011. The standard contains three new solid solution strengthened ferritic ductile iron grades: 450–18, 500–14 and 600–10. There are some studies for laboratory scale SSF samples, but very few studies about actual full scale SSF ductile iron production. The objective of this thesis was to gain more insight about the specifics of SSF ductile iron production.

The theory portion of this thesis consists of a literature survey that focuses on cast iron metallurgy, ductile iron melt processes and cooling curve analysis of cast irons. The experimental part of this thesis consists of two production trials of 600–10 ductile iron and several linked cooling curve analyses and solidification simulations.

The production trials were not completely successful. Different separately cast tensile test bars showed properties above and below standard requirements. Cooling curve samples taken during the trials showed that more potent nodulant and inoculant materials might be needed for production of 600–100 SSF ductile iron grades. The solidification simulations showed that the software does not fully understand the properties of the SSF grades, but it still is a useful tool for ductile iron design.

TIIVISTELMÄ

OLLI PARTANEN: Liuoslujitettujen pallorautagrafiittivalurautojen valmistuksen optimointi jäähtymiskäyräanalyysillä ja jähmettymissimuloinnilla
Tampereen teknillinen yliopisto
Diplomityö, 53 sivua
Huhtikuu 2016
Materiaalitekniikan koulutusohjelma
Pääaine: Metallimateriaalit
Tarkastajat: Dos. Juhani Orkas ja Assoc. Prof. Pasi Peura
Avainsanat: GJS 600–10, pallografiittivalurauta, liuoslujittuminen, jäähtymiskäyräanalyysi, jähmettymissimulointi

Uusin pallografiittivalurautoja käsittelevä EN standardi 1563 ilmestyi vuonna 2011. Siinä esiteltiin kolme uutta piillä liuoslujitettua ferriittistä laatua: 450–18, 500–14 ja 600–10. Näiden materiaaliominaisuuksista löytyy joitain materiaalitutkimuksia, mutta toistaiseksi näistä laaduista valmistetuista teollisen mittakaavan valuista on tehty hyvin vähän tutkimusta. Tämän diplomityön tarkoitus oli tarkemmin tutkia näiden laatujen teollisen valmistuksen yksityiskohtia.

Diplomityön teoriaosuus käsittelee valurautojen metallurgiaa, rautavalimon sulaprosessia sekä valurautojen jähmettymiskäyräanalyysiä. Työn kokeellisessa osuudessa valmistettiin vetokoesauvoja 600–10 materiaalista, sekä tutkittiin valmistuksen yksityiskohtia jäähtymiskäyräanalyysillä ja jähmettymissimuloinneilla.

Koevaluista saatiin ristiriitaisia tuloksia. Eri käsittelyaineilla valmistetuista vetokoesauva-aihioista osa jäi standardin vaatimusten alapuolelle, kun taas osa selkeästi ylitti vaatimukset. Koevalujen aikana otettujen jäähtymiskäyräanalyysien perusteella teisteissä käytetyt palloutus- ja ymppäysaineet eivät välttämättä ole riittävän voimakkaita 600–10 laadun valmistukseen. Jäähtymissimulointiohjelmisto ei näytä vielä täysin ymmärtävän liuoslujitettujen pallografiittilaatujen ominaisuuksia, mutta se on silti hyödyllinen työkalu niiden suunnitteluun.

PREFACE

This thesis was done as the final part of my studies for Master of Science (Technology) degree in Materials Engineering at Tampere University of Technology.

First I would like to thank Componenta Oyj for this thesis topic and for the start I have received to my engineering career. This thesis was a part of FIMECC's Breakthrough Steels and Applications subproject Novel Cast Materials. I would like to thank FIMECC for its contributions to my thesis project.

From Componenta I would like to thank my instructors M.Sc. (Tech), M.Sc. (Econ.) Ilkka Harri and M.Sc. (Tech) Tony Pitkänen for their help and criticism of my thesis. I would also like to thank my supervisors from the Department of Materials Science of Tampere University of Technology, Docent Juhani Orkas and Associate Professor Pasi Peura.

Finally, thanks to all my friends and family for making the journey worthwhile.

Tampere, April 9th 2016

Olli Partanen

TABLE OF CONTENTS

LIST OF FIGURES

LIST OF TABLES

LIST OF ABBREVIATIONS AND SYMBOLS

A1	Lower critical temperature
BCC	Body centered cubic
CCA	Cooling curve analysis
CE	Carbon equivalent
CHG	Chunky graphite
EAF	Electric arc furnace
FCC	Face centered cubic
FDM	Finite difference method
FEM	Finite element method
FVM	Finite volume method
GJS	Ductile iron, spheroidal graphite cast iron
HET	High eutectic temperature
LET	Low eutectic temperature
LT	Liquidus temperature
R	Recalescence
RE	Rare earth
SSF	Solid solution strengthened ferritic
ST	Solidus temperature
wt%	Mass fraction

1. INTRODUCTION

Even though the production of ductile irons was invented in the 1950s, new improvements to ductile iron production are still being made today. Solid solution strengthened ferritic (SSF) ductile iron grades are a relatively new material. Even though some solid solution strengthened ductile iron grades have been known since at least the 1990s, the European EN standard that includes the modern SSF grades was published in 2011. Even though the standard is several years old and there have been studies showing the material properties of SSF ductile iron in test specimen scale, there are very few studies that show the properties and problems of SSF castings in normal foundry production scale. Cooling curve analysis and solidification simulation are common tools used in cast iron design and foundry process evaluation. Main purpose of this thesis was to study the specifics of 600–10 grade SSF ductile iron production. The use of cooling curve analysis and solidification simulation are linked to various production steps to gain deeper understanding of the process.

This thesis starts with introduction to the theory behind cast iron metallurgy, foundry processes relevant for ductile iron production, cooling curve analysis and solidification simulation of cast iron. This is followed by description of the tests done for this thesis, their results and finally discussion about the results. Some suggestions for further research are given as well.

2. THEORETICAL BACKGROUND

This chapter discusses the theoretical background of cast irons, focusing on metallurgy and properties of cast irons and parts of melt treatment process important for cast iron production. This theory portion of this thesis does not describe all types of cast irons or every phenomena regarding cast iron metallurgy. The focus of this thesis is on ductile irons and more specifically solid solution strengthened ferritic grades of ductile iron.

2.1 Cast iron metallurgy

This section focuses on metallurgy of cast irons, specifically to ductile iron metallurgy. This section focuses on properties that are common with several types of cast irons, properties of the solid solution strengthened ferritic ductile iron grades are discussed in Section 2.2.

2.1.1 Fe-C phase diagram

The iron-carbon phase diagram consists of two different systems: metastable iron-cementite system and stable iron-graphite system. Both systems are shown in Figure 2.1. Steels and white cast irons should have a Fe-Fe_3C microstructure and cast irons, excluding white irons, should have a Fe-graphite microstructure. The metastable system is still important for cast irons, as fast cooling and some alloying elements can promote cementite formation, which is detrimental for cast irons. [12]

The main difference between cast irons and steels is that cast irons have more than 2.1 wt% of carbon. Below this carbon content iron always solidifies completely as austenite before forming other microstructures. Above this carbon content the liquid iron that has not yet solidified as austenite, undergoes an eutectic reaction at about 1150 ℃, solidifying as both austenite and graphite at the same time. If the

composition of the iron is at the eutectic point 4.3 wt% carbon or carbon equivalent, the iron solidifies at one specific temperature and there is no semisolid state where both solid and liquid state are in equilibrium at the same time. [12, 15]

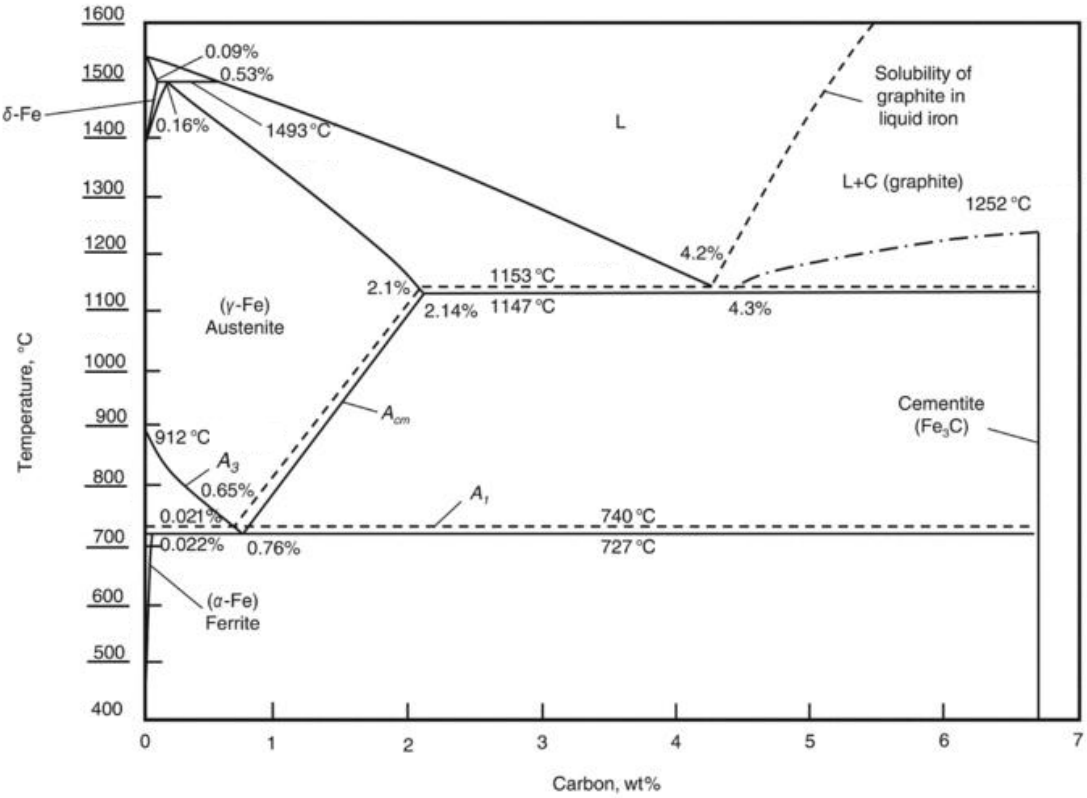

Figure 2.1 *Iron-carbon phase diagram. Solid lines indicate metastable Fe-Fe_3C system, dashed lines indicate stable Fe-graphite system. Adapted from [11].*

It should also be noted that the Fe-C phase diagram tells the equilibrium microstructure of a iron-carbon binary system. It cannot be used to determine the microstructure of cast iron parts by itself, as reaching equilibrium would require infinitesimal cooling rates [15]. Cast irons contain several alloying elements which change the shape of the phase diagram and there are also several liquid treatments and heat treatments that affect the final microstructure of cast iron parts. [12]

2.1.2 Carbon equivalent

Carbon equivalent (CE) is a parameter that affects microstructure, mechanical properties and castability of cast irons. Carbon equivalent takes into account elements

that have similar effect as carbon on the eutectic composition [15]. Typically silicon and phosphorus are considered when calculating carbon equivalent. This concept for carbon equivalent should not be confused with the concept used for evaluating weldability of steel, which is also abbreviated as CE.

There are several ways of calculating carbon equivalent for cast irons. A common way is shown in Equation 2.1.

$$CE = \%C + \frac{1}{3}(\%Si + \%P) \tag{2.1}$$

Here CE is carbon equivalent and $\%C$, $\%Si$ and $\%P$ are carbon, silicon and phosphorus contents as wt%, respectively. Some versions of the equation also include manganese and sulfur. If carbon equivalent is 4.3 the composition of cast iron is eutectic and it solidifies completely as an eutectic austenite-graphite structure. This corresponds to the point at 4.3 wt% carbon and at about 1150 ℃ in binary iron-carbon system as seen in Figure 2.1. If carbon equivalent is below 4.3 the cast iron solidifies first as primary austenite before the eutectic reaction starts. If carbon equivalent is above 4.3 the first phase to form is primary graphite. [12, 22].

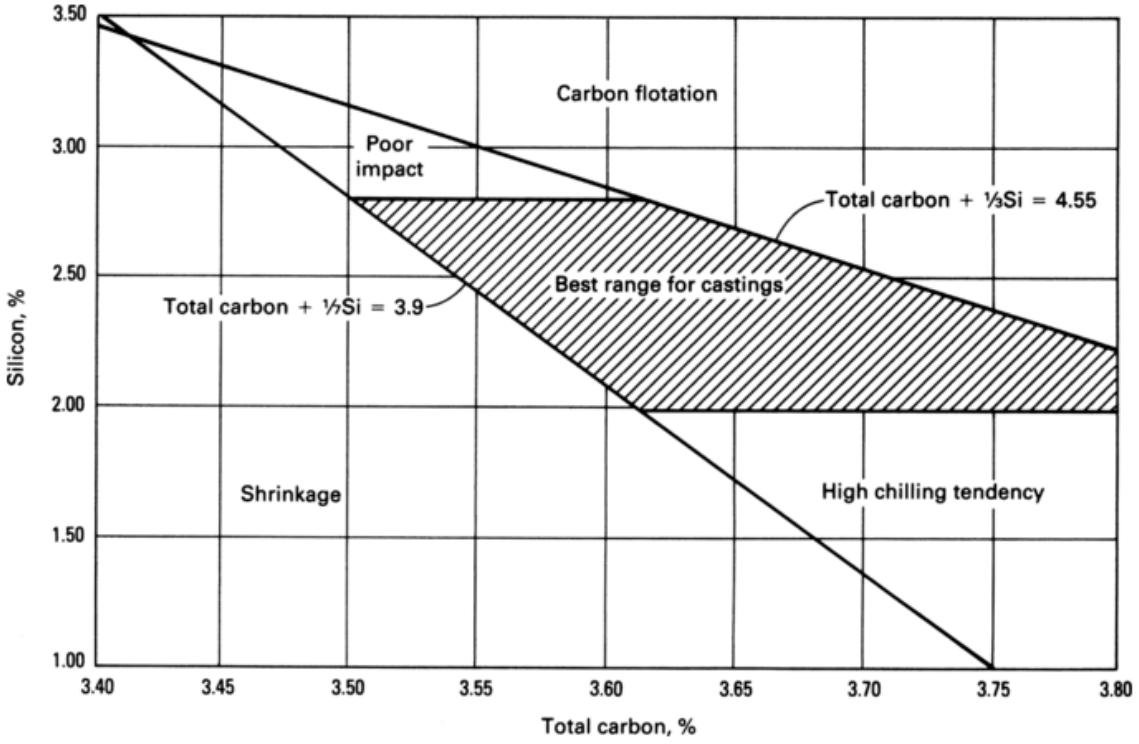

Figure 2.2 *Effect of carbon and silicon contents on conventional ductile iron mechanical properties and castability [10]*

Higher carbon equivalents can lead to better castability, because there should be more graphite formation which counters shrinkage. However, excess formation of primary graphite can lead to graphite flotation, which is detrimental for mechanical properties of the upper part of the casting, as the localized graphite content increases. So carbon equivalent of cast iron parts is usually near eutectic to optimize castability and mechanical properties. This is illustrated in Figure 2.2, which shows the effect of carbon and silicon contents on properties of ductile iron. [10, 12]

2.1.3 Alloying elements in cast iron

Alloying elements in cast irons can be divided into three categories: primary, alloying and trace. The distinction between these groups is not completely unambiguous, as different properties are desired in each type of cast iron. Also, the effect an element has on properties of cast iron can depend on concentration and how the element interacts with other elements. Primary elements, carbon, silicon, manganese, phosphorus and sulfur are present in all cast irons. Alloying elements are added to

modify the properties of cast irons. Common elements in cast irons and their effects are summarized in Table 2.1. Trace elements are not deliberately added, they come from raw materials as impurities. The amount of harmful trace materials is usually kept at sufficiently low levels, as it is difficult to completely remove them from the melt. [10, 15]

As mentioned in Section 2.1.2, carbon content influences the microstructure of cast irons and the amount of graphite formation. Silicon, another element used to calculate carbon equivalent, forms solid solution with iron matrix. This strengthens the matrix and also decreases the solubility of carbon in the matrix, which causes more graphite to precipitate [25]. Silicon promotes ferrite formation and excess amounts of silicon can cause brittleness in cast irons. Phosphorus is included in calculating carbon equivalent. Small amounts of phosphorus can form a solution with ferrite, which increases strength and hardness. Excess phosphorus segregates, which lowers elongation and causes brittleness. [10]

Manganese and sulfur contents should be considered relative to each other, as sulfur has a tendency to form either FeS (iron sulfide) or MnS (manganese sulfide). FeS forms at grain boundaries and it can cause white solidification. MnS is a harmless compound and it distributes uniformly throughout the matrix. Sulfur also forms MgS (magnesium sulfide) with magnesium added to ductile irons, so excess sulfur can lead to failed nodularization treatments. The manganese that does not form MnS acts as an alloying element and it promotes pearlite and carbide formation. Manganese levels of over 1 wt% can cause white solidification, so it is important to keep sulfur levels low rather than to add manganese to counter the effects of sulfur. Use of steel scrap as raw material needs to be controlled, as steel can contain relatively high amounts of manganese. [10, 15]

Table 2.1 *Effect of alloying elements on cast iron matrix and graphite formation. Adapted from [10, 25].*

Element	Effect on graphite formation	Effect on eutectoid reaction
Al	Strong graphitizer	Promotes ferrite
B (<0.015%)	Strong graphitizer	Promotes graphite formation
B (>0.015%)	Carbide stabilizer	Strong pearlite retainer
Bi	Carbide promoter	Very mild pearlite stabilizer
Cu	Mild graphitizer	Promotes pearlite formation
Cr	Strong carbide former	Strong pearlite former
Mn	Mild carbide former	Pearlite former
Mo	Mild carbide former	Promotes pearlite formation
Ni	Graphitizer	Mild pearlite promoter
Sb	Little effect in amount used	Strong pearlite stabilizer
Si	Strong graphitizer	Promotes ferrite and graphite formation
Sn	Little effect in amount used	Strong pearlite promoter and retainer
Te	Very strong carbide promoter	Very mild pearlite stabilizer
Ti (<0.25%)	Graphitizer	Promotes graphite formation
V	Strong carbide former	Strong pearlite former

Common alloying elements in cast irons include chromium, copper, molybdenum, nickel, tin and vanadium, also magnesium for ductile irons. Out of these, nickel, copper and tin act as pearlite promoters in increasing order of efficiency. Copper and nickel also promote graphite formation. Copper is commonly used for the stronger, pearlitic grades of ductile iron. Small amounts (<0.1 wt%) of tin can also be used to achieve fully pearlitic matrix. [10, 15]

Molybdenum, chromium and vanadium are carbide promoters, in increasing order of potency. At low contents they increase strength by promoting pearlite formation. So the levels of these elements need to be controlled to prevent white solidification in ductile iron production. The mechanisms for promoting either graphite or carbide promotion are discussed further in Section 2.1.6. [15]

Trace elements in cast irons include aluminum, antimony, arsenic, bismuth, boron, cerium, lead, tellurium and titanium. Many trace elements are pearlite and carbide promoters (e.g. B, Bi), so a high purity melt is required for fully ferritic grades and to prevent white solidification. Some of these elements also negatively effect the shape of graphite: lead can cause the formation of spiky graphite in cast irons (decreases strength) and antimony can stop carbon from diffusing into graphite nodules in ductile iron, which causes lamellar graphite formation (decreases strength and elongation). However, sometimes small amounts of trace elements can be added to the melt on purpose. For example, small additions ($<$0.005 wt%) of cerium, which by itself in excessive amounts can cause chunky graphite formation, can counter the negative effects of other trace elements. [10, 15, 25]

2.1.4 Phases in cast iron

Austenite (γ-iron) is the first matrix phase to form as cast iron solidifies. It decomposes into other phases during cooling, but with certain heat treatments and alloying elements austenite can remain stable at room temperature. Austenite has a FCC (face centered cubic) crystal structure and the maximum solubility of carbon into iron (2.1 wt%) occurs at 1150 ℃. This solubility decreases as temperature drops, at lower critical temperature (A1) the solubility is only 0.8 wt%. All other matrix phases in cast irons form from austenite during cooling (excluding heat treatments done after casting) and the composition of austenite has an effect on the properties of other phases as well. [12, 29]

Ferrite (α-iron) is a phase of almost pure iron. Ferrite is stable at room temperature and it has a BCC (body centered cubic) crystal structure. Solubility of carbon into ferrite is only 0.02 wt% at its highest (at A1 temperature) and at room temperature the solubility is reduced to below 0.005 wt%. [5] Ferrite has high ductility and toughness but relatively low strength. Ferrite forms at low cooling temperatures and some alloying elements, such as silicon for cast irons, promote ferrite formation. A ferritic microstructure can also be achieved with heat treatments. Ferritic ductile iron is shown in Figure 2.3. [15]

Pearlite is a lamellar structure that consists of ferrite and cementite (Fe_3C) phases. Compared to ferrite, pearlite has higher strength values with subsequent decrease in elongation. Pearlite forms at higher cooling rates than ferrite and as with ferrite,

some elements (e.g. copper) promote pearlite formation and a pearlitic microstructure can also be achieved with heat treatments. [10, 15]

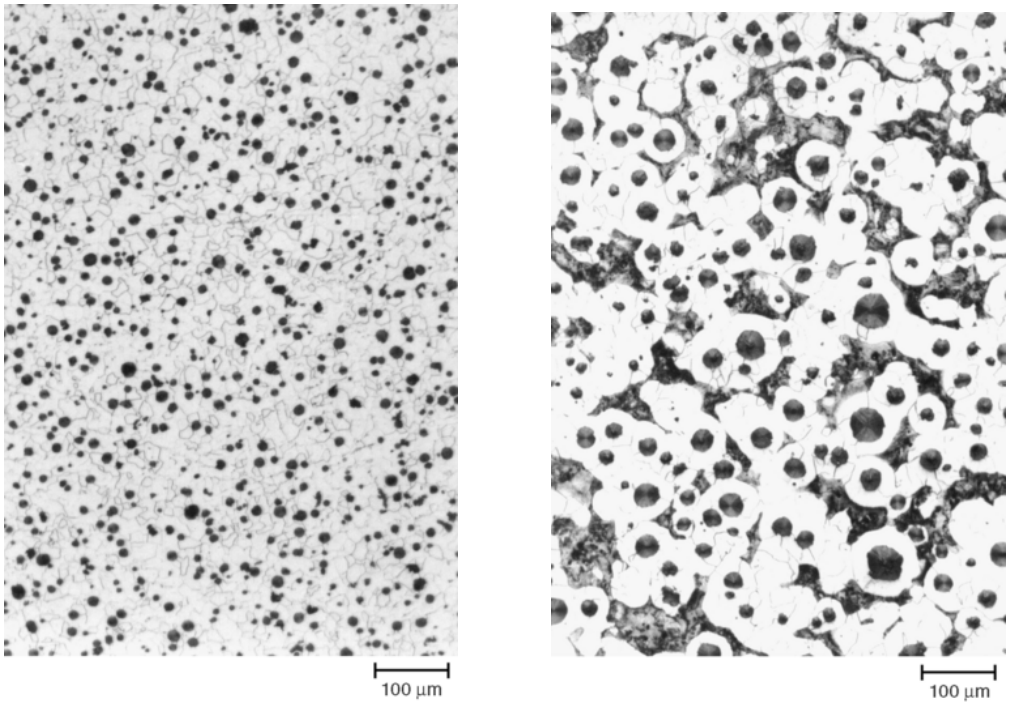

(a) Completely ferritic microstructure.

(b) Ferritic-pearlitic microstructure. Ferrite shells around graphite nodules surrounded by pearlite.

Figure 2.3 *Ductile iron microstructures. [7]*

Usually the microstructure of conventional as-cast cast iron parts is neither fully ferritic or pearlitic, but a combination of both. The areas near graphite particles are usually fully ferritic, as carbon diffuses into the particle. Pearlite forms in the areas in between the graphite particles, as there is not enough time for the carbon in cementite to diffuse to the graphite particles during normal cooling. This type of cast iron is shown in Figure 2.3. [29]

2.1.5 Graphite morphology

Cast irons are classified by their by the shape of graphite particles present in the iron. EN ISO standard 945 "Microstructure of cast irons - Part 1: Graphite classification

by visual analysis" gives six different principal forms in cast irons and further several reference pictures for shape and size within each of the principal types. The principal graphite forms are shown in Figure 2.4. Their descriptions are presented in Table 2.2, focusing on graphite forms present in ductile irons.

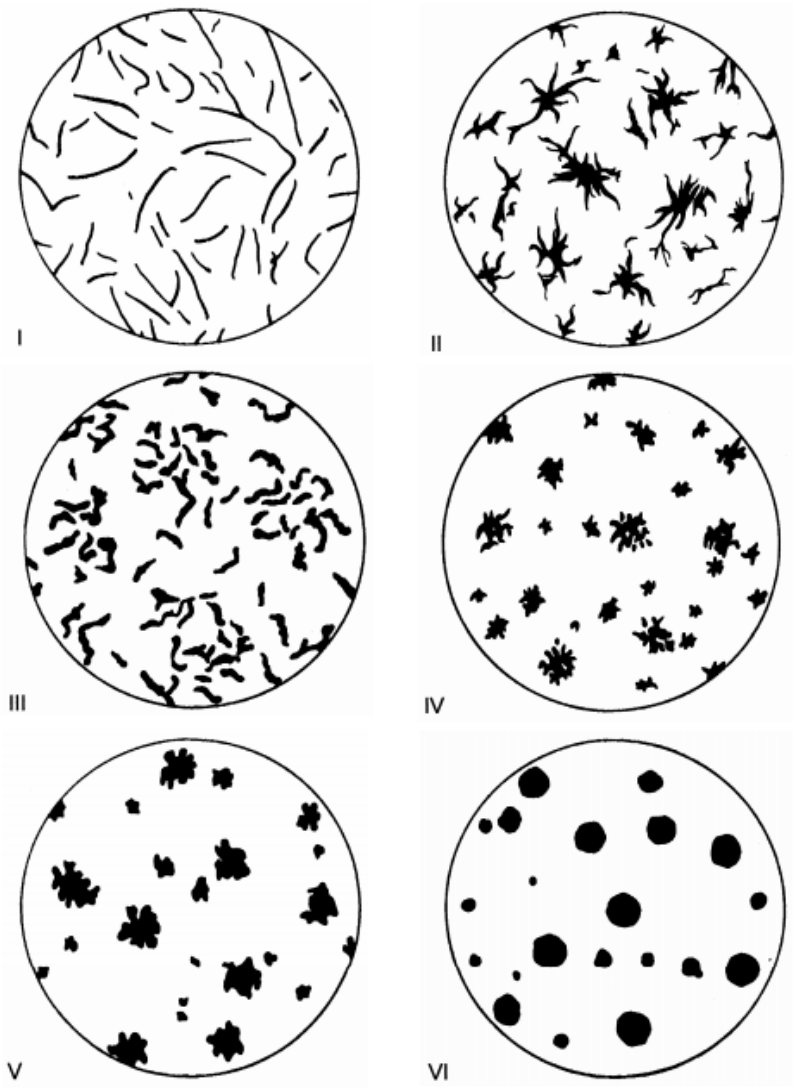

Figure 2.4 *Principle graphite forms of EN 945. [4]*

Table 2.2 *Description of graphite forms of EN 945. Adapted from [4]*

Form	Name of graphite form	Main characteristics	Occurrence
I	Lamellar (flake) graphite	Lamellar graphite with sharp ends	Principal form in gray iron
II	Crab graphite	Aggregate of graphite flakes	Can occur in rapidly cooled gray irons or thick walled ductile iron
III	Compacted graphite	Worm like with round ends	Can occur in ductile iron
IV	Irregular spheroidal graphite	Isolated particles	Can occur in ductile iron
V	Slightly irregular spheroidal graphite	Isolated particles	Principal form in thick-walled ductile iron
VI	Spheroidal graphite	Isolated particles	Principal form in ductile iron

Type VI is the desired graphite shape in ductile irons. Other graphite types are defects in ductile irons, with the exception of type V in thick walled castings. However, EN ISO standard 1563 "Founding - Spheroidal graphite cast irons" does not dictate the required graphite shape in ductile iron castings, as long as the mechanical properties are met [1]. The standard recommends nodularity (presence of forms V and VI) of 80 %. Castings with heavy sections are more susceptible to imperfect nodules, as the effect of nodularization and inoculation start to fade with longer cooling times. There are also several other detrimental graphite shapes in addition to the ones mentioned in EN 945 standard. Figure 2.5 shows two other detrimental graphite forms: chunky graphite and exploded graphite.

Chunky graphite (CHG, shown in Figure 2.5) is a detrimental graphite structure commonly found in ductile iron castings that have large sections or that are made from high purity raw materials. The formation mechanism of CHG is not completely understood, but there are several theories. However, many possible culprits for CHG formation are known. These are large section size and the following elements: Ce

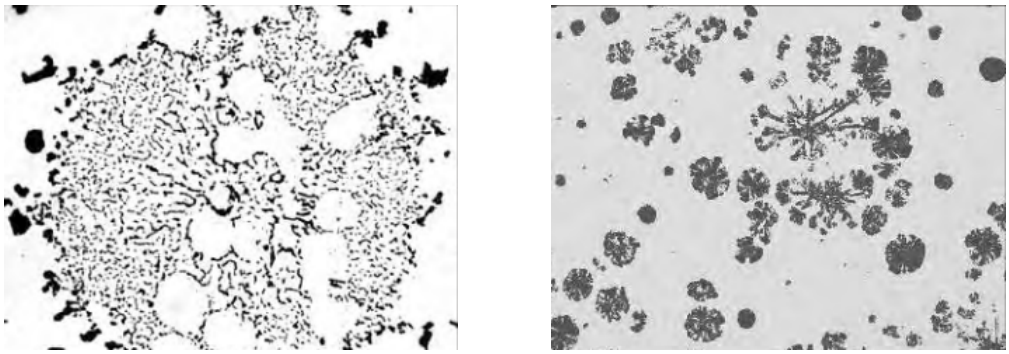

(a) Chunky graphite (b) Exploded graphite

Figure 2.5 *Nonstandard detrimental graphite forms [8].*

and other rare earth (RE) elements, Ca, Ni, Si, Al and Mg [24, 26, 30]. Many of these elements, such as Ca and Ce are not added as an alloying element to base iron, but they are present in inoculant materials.

Cerium and other RE elements are commonly thought to be the main reason behind CHG formation [19, 30]. These are added to the iron melt as part of inoculation materials and in in other types of cast irons they can be used to counter other detrimental graphite shapes [15]. Small addition of antimony to the melt can be used to counter CHG formation [19, 24, 27]. Some other elements, such as bismuth also have a similar counteracting effect on CHG formation [24]. The addition of the elements should be limited, as they too cause other detrimental graphite shapes if added in excess.

Presence of CHG is highly detrimental for mechanical properties of ductile iron. When CHG is present, yield strength is mostly unaffected, but tensile strength and elongation are greatly reduced [20]. This phenomenon is obvious in a tensile test, but can be dangerous in an actual casting if it goes unnoticed. As CHG formation is promoted by large section sizes, CHG might not be present in a separately cast tensile test specimen but the mechanical properties of the actual, larger casting might be greatly lowered by CHG formation.

2.1.6 Solidification of cast iron

Cast irons have three different solidification types depending on carbon equivalent: hypoeutectic, eutectic and hypereutectic solidification. Out of these three, eutectic solidification occurs with all cast irons, as they all eventually reach eutectic transformation temperature. If the composition of cast iron is eutectic (CE 4.3) the solidification will be completely eutectic. The first phase to form in hypoeutectic cast irons is primary austenite and for hypereutectic cast irons it is primary graphite. Figure 2.6 shows the formation of hypereutectic ductile iron, which starts with precipitation of primary graphite nodules and is followed by eutectic formation of both austenite dendrites and graphite nodules. Figure 2.6 also illustrates a cooling curve for cast iron solidification, which is a useful tool for cast iron production and it is further discussed in Section 2.4. [10]

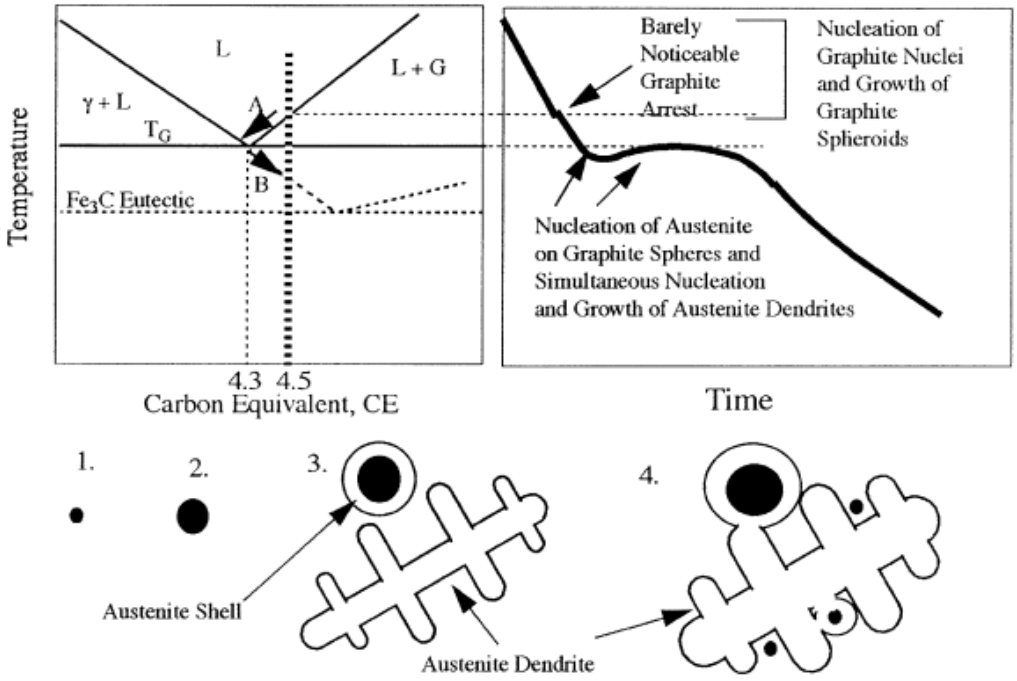

Figure 2.6 *Solidification and cooling curve of hypereutectic cast iron [6].*

Both austenite and carbon solidify at the same time during eutectic solidification. The carbon phase is determined by the amount of undercooling. In pure iron-carbon binary system the eutectic temperatures for graphite and cementite formation are very close to each other, as seen in Figure 2.1. However, the silicon present in cast irons significantly lowers the eutectic temperature for cementite formation which

causes carbon to solidify as graphite under normal cooling conditions [6]. Despite of this, high cooling rates and some alloying elements can lead to significant undercooling and white solidification. [10]

In ductile irons graphite nodules and austenite dendrites start to solidify at the same time, independent of each other. This is illustrated in Figure 2.6, at stages 3 and 4. The graphite nodules create favorable conditions for austenite formation around of them. So in additions to dendrites, austenite also forms shells around graphite nodules as the melt near the nodules is depleted of carbon. This mechanism is illustrated in Figure 2.7, which shows different stages of graphite nodule formation. [10]

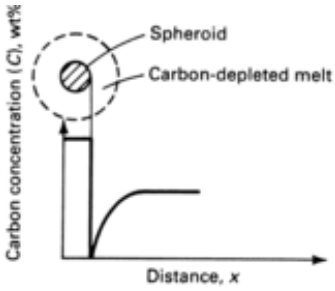

(a) Precipitation of graphite nodule in liquid iron.

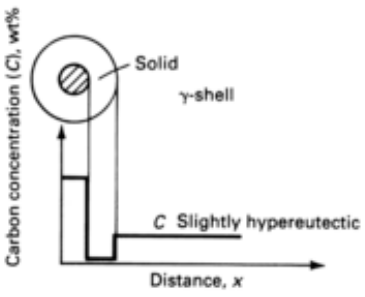

(b) Solidification of austenite shell around graphite nodule.

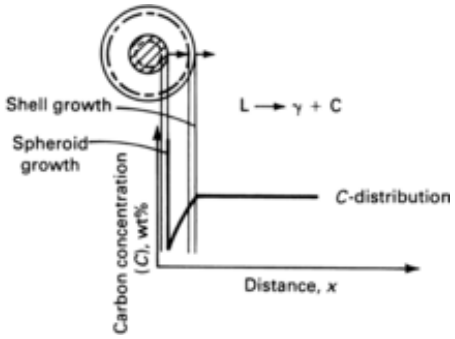

(c) Growth of graphite nodule by carbon diffusion through austenite shell.

Figure 2.7 *Growth of graphite nodule with austenite shell. Adapted from [10].*

The carbon content of austenite is at its maximum right after eutectic solidification. Subsequent cooling causes changes in the microstructure as carbon starts to precipitate out of austenite. Chemical composition and cooling rate are the main variables for final matrix microstructure. The size, shape and distribution of the car-

bon particles right after solidification also affect final microstructure of the casting. [10]

Some elements (e.g. Cu, Sn) segregate near the surface of graphite particles and act as diffusion barriers. These elements act as pearlite promoters. This does not occur with all pearlite promoting elements, some segregate to intercellular areas [14]. These elements (e.g. Cr, V) also have a tendency to form free intercellular carbides so excess amounts of these elements should be limited to avoid free carbide formation. Silicon promotes ferrite formation by raising the upper critical temperature, causing the transformation from austenite to ferrite to happen at a higher temperature with faster carbon diffusion [6]. Some elements (e.g. Cu, Ni) promote graphite formation by increasing the difference between stable and metastable eutectic temperatures or by reducing solubility of carbon in austenite, causing more carbon to diffuse to the graphite particles. [10, 25]

2.1.7 Solid solution strengthening

Solid solution strengthening is one of the main strengthening mechanism in metals. Alloys that form solid solution are stronger than pure metals, as the impurity or solute atoms cause lattice strains in the surrounding matrix. These strains impede dislocation movement, thus making the material stronger. This increase in material strength is accompanied by decrease in ductility [17]. There are two types of solute atoms: substitutional and interstitial. Substitutional solute atoms substitute the solvent atoms and interstitial solute atoms occupy the empty space between solvent atoms. These two different solid solution types are illustrated in Figure 2.8.

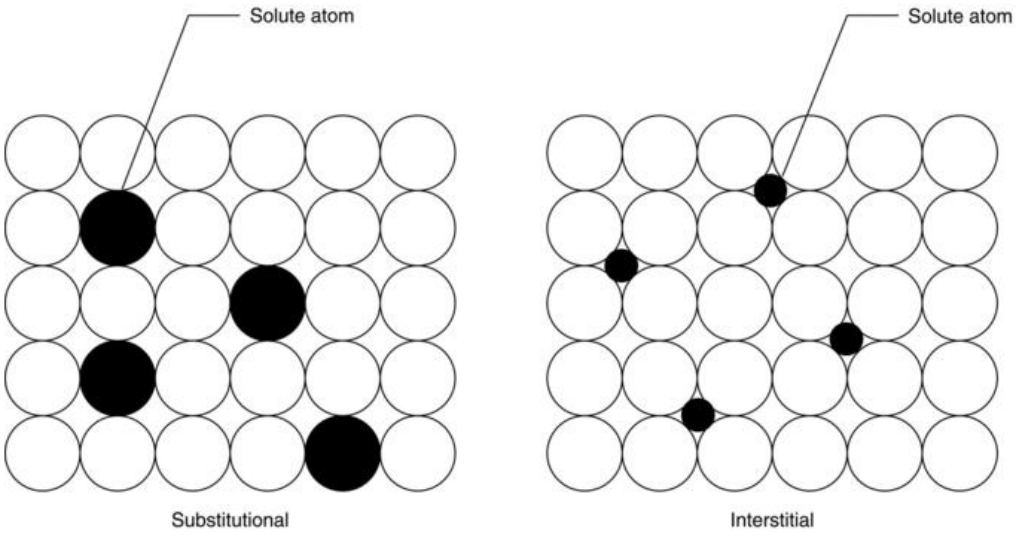

Figure 2.8 *Substitutional and interstitial solute atoms. [11]*

Several characteristics are involved in solid solubility of different metal atoms. For substitutional atoms, same crystal structure and similar atomic size, electronegativity and valency as with the solvent atoms increase solubility. Interstitial solute atoms need to be small to fit to the interstices between atoms and similar electronegativity also increases the solubility of interstitial atoms [17]. Several elements act as solid solution strengtheners in cast irons, as discussed in Section 2.1.3. The solid solution strengthening effect of several elements is illustrated in Figure 2.9, which shows the effect of dissolved alloying elements on the yield stress of ferrite. It should be noted that this figure shows the effect of dissolved solute atoms, not the total weight fraction of an element.

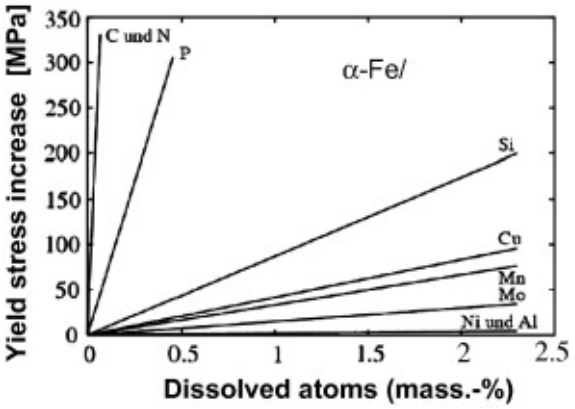

Figure 2.9 *Effect of several solid solution forming elements on yield strength of ferrite. [31], see [32].*

2.2 SSF ductile iron grades

This section focuses on the properties on solid solution strengthened ferritic ductile iron grades, mainly on the mechanical properties and chemical composition of these grades.

2.2.1 Mechanical properties of SSF ductile iron

Ductile iron grades have standardized names that indicate the tensile strength and elongation (in MPa and percentage, respectively) of a tensile test specimen, e.g. EN-GJS-600-10. It should be noted that these values are given for separately cast samples of relatively small wall thickness (below 30 mm). The requirements decrease as the wall thickness increases and these requirements for SSF grades of ductile iron from EN standard 1563 are shown in Figure 2.10. The requirements for mechanical properties also change if the tensile specimen is taken from the actual casting and these mechanical requirements are shown in Figure 2.11. For example, a tensile test bar taken from a casting with relevant wall thickness of 50 mm made from EN-GJS-600-10 only needs to have tensile strength of 560 MPa and elongation of 6 % to meet the standard. [1]

Material designation		Relevant wall thickness	0,2 % proof strength	Tensile strength	Elongation
Symbol	Number	t mm	$R_{p0,2}$ MPa min	R_m MPa min	A % min
EN-GJS-450-18	5.3108	$t \leq 30$	350	450	18
		$30 \leq t \leq 60$	340	430	14
		$t > 60$	to be agreed upon between the manufacturer and the purchaser		
EN-GJS-500-14	5.3109	$t \leq 30$	400	500	14
		$30 \leq t \leq 60$	390	480	12
		$t > 60$	to be agreed upon between the manufacturer and the purchaser		
EN-GJS-600-10	5.3110	$t \leq 30$	470	600	10
		$30 \leq t \leq 60$	450	580	8
		$t > 60$	to be agreed upon between the manufacturer and the purchaser		

Figure 2.10 *Mechanical properties of SSF ductile irons from EN 1563. Separately cast samples. [1]*

Material designation		Relevant wall thickness	0,2 % proof strength	Tensile strength	Elongation
		t	$R_{p0,2}$	R_m	A
		mm	MPa	MPa	%
Symbol	Number		min.	min.	min.
EN-GJS-450-18C	5.3108	$t \leq 30$	350	440	16
		$30 < t \leq 60$	340	420	12
		$60 < t \leq 200$	Guidance values to be provided by the manufacturer		
EN-GJS-500-14C	5.3109	$t \leq 30$	400	480	12
		$30 < t \leq 60$	390	460	10
		$60 < t \leq 200$	Guidance values to be provided by the manufacturer		
EN-GJS-600-10C	5.3110	$t \leq 30$	450	580	8
		$30 < t \leq 60$	430	560	6
		$60 < t \leq 200$	Guidance values to be provided by the manufacturer		

Figure 2.11 *Mechanical properties of SSF ductile irons from EN 1563. Samples cut from castings. [1]*

In addition to the increased elongation compared to conventional ductile irons of similar strength values, SSF ductile irons also have several other benefits. First, due to their uniform ferrite matrix they have smaller hardness variations than the convention grades that contain both ferrite and pearlite, which is beneficial for improved machining tool life expectancy. Second, SSF grades have higher yield strength/tensile strength ratio than conventional grades: 75-85 % vs. 55-65 %, respectively. This increase in yield strength allows for lighter or stronger components. [1]

2.2.2 Chemical composition of SSF ductile iron

SSF ductile irons are mainly alloyed by additional silicon compared to conventional grades. Silicon strengthens and stabilizes ferrite. Other elements (P, Mn, etc.) also act solid solution strengtheners, but they tend to have harmful effects so they cannot be used as the main alloying element for solid solution strengthening. EN standard 1563 gives guidelines for chemical composition for SSF ductile iron grades, these are shown in Figure 2.12. As the composition of most castings should be near eutectic composition, the carbon levels are increasingly lower with stronger grades. [1, 10]

The matrix of SSF ductile irons should be mostly ferritic, but the EN 1563 standard allows for up to 5 % pearlite. The addition of silicon is slightly detrimental to the shape of the graphite nodules, but at the same time the strengthened ferrite matrix is less sensitive graphite nodule defects. So the standard allows approximately 20 % of compacted graphite (form III, Figure 2.4), as long as the rest of the nodules are

spheroidal. Nodularity of 80 % is not a mandatory value by itself, so castings can have even lower nodularity if the mechanical properties are met. [1]

Designation		Si	P	Mn
Symbol	Number	% approx. [a]	% max.	% max. [b]
EN-GJS-450-18	5.3108	3,20	0,05	0,50
EN-GJS-500-14	5.3109	3,80	0,05	0,50
EN-GJS-600-10	5.3110	4,30	0,05	0,50

[a] Si content may be lower due to other alloying elements.
[b] With lower Mn content (e.g. 0,30 %), machinability and elongation will be improved.

Figure 2.12 *Guidelines for SSF ductile iron chemical compositions from EN 1563. [1]*

EN 1563 suggests silicon content up to 4.3 wt% for the strongest SSF grade, 600–10. 4.3 – 4.5 wt% of silicon is the upper limit of silicon that should be added, as this is the point where yield and tensile strengths reach their maximum and elongation values start to drastically decrease. Other alloying elements also have an effect of this, for example 0.6 wt% Cr can significantly lower elongation values at just 4.0 wt% of silicon. [35]

2.3 Ductile iron foundry process

Every part of the foundry process is important for making sound castings, but this thesis focuses on melting and melt treatment stages that are specifically important for making SSF ductile iron castings. Other stages, such as molding and core production remain largely the same regardless of the type of cast iron being produced. Figure 2.13 shows a typical melt process of a ductile iron foundry, starting with melting of raw materials. Then the melt is magnesium treated, typically with a FeSiMg alloy. Inoculation is usually done in two steps: first by adding inoculant to the ladle or the melt stream when tapping from the furnace to the ladle and also to the mold or the melt stream during pouring.

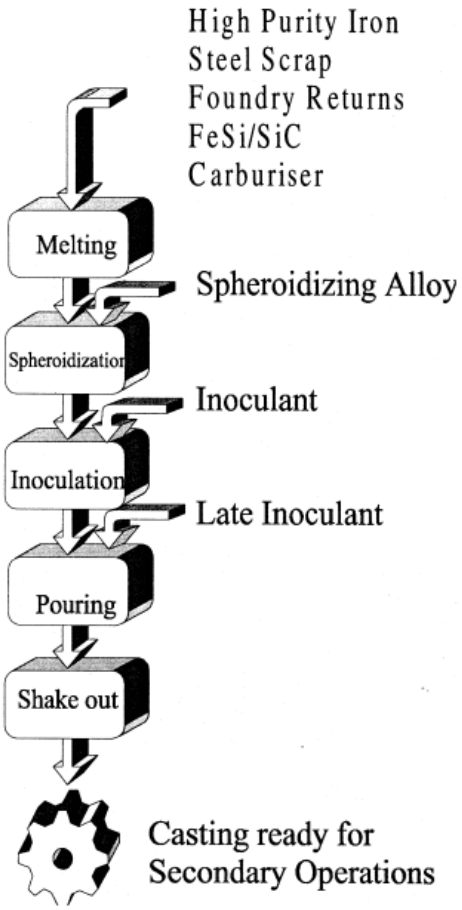

Figure 2.13 *Melt process of ductile iron production [25].*

2.3.1 Melting

The three main furnace types for melting cast iron are cupola furnaces, electric arc furnaces and induction furnaces. Modern cupola furnaces were invented in late 18th century and they were the main method for iron melting for several hundred years, until electric furnaces started to become common in the 1950s. [10]

Fundamentally a cupola is a cylindrical furnace that uses coke as a source of heat. The cylinder is alternately charged with coke and iron raw material (steel and cast irons scrap, pig iron, etc.) and air is blown to the cupola to burn the coke. The heat from burning coke melts the iron and the molten iron is collected at the bottom of the cylinder. The molten iron can be continuously poured from the cupola or it can be periodically tapped. The temperature of the molten iron can be controlled by the air flow, but cupola furnaces are still less effective at superheating molten

iron than electric furnaces. The iron also reacts with the carbon in coke, so there is some process variation in the carbon content of the melt. Despite these drawbacks, cupola furnaces are the most cost efficient furnace in foundries with high tonnage production, where the grade of iron being produced is not changed often. [10, 15]

Electric furnaces, electric arc furnaces (EAFs) and induction furnaces melt iron with electric current, no additional fuel source is needed. Compared to cupola furnaces, electric furnaces offer better control of melt temperature and composition. EAFs melt metal by forming an electric arc between the furnace electrodes and metal charge and induction furnaces form eddy currents in the metal charge. Out of these two processes, induction furnaces are more popular in cast iron production where relatively small batches of different grades are produced, compared to EAFs that are more common in steel production where larger batches are common. Induction furnaces also provide better superheating capabilities ant tapping temperature control. [10, 15]

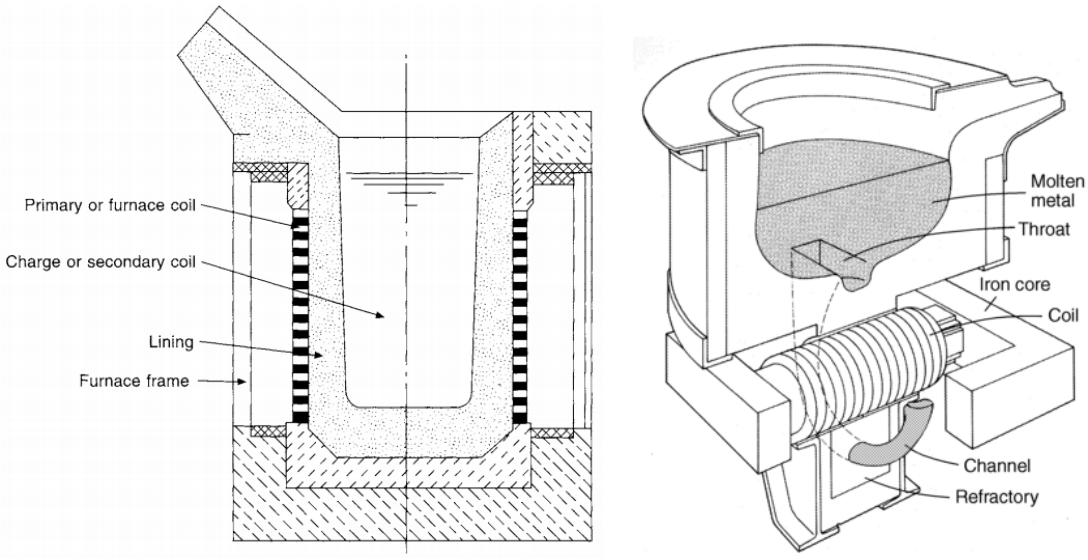

(a) Coreless furnace [16]. (b) Channel furnace [5].

Figure 2.14 *Illustrations of induction furnaces.*

Induction furnaces can be used for both melting and holding of molten iron. There are two main types of induction furnaces: coreless and channel. Coreless induction furnace has coil surrounding the entire metal charge whereas channel furnaces have an induction loop in the bottom of the furnace. These two types of induction fur-

naces are illustrated in Figure 2.14. While in the channel furnace the coil only heats a small portion of the melt, the stirring effect of eddy currents keeps temperature and composition of the melt uniform. The channel furnace needs to have a certain level of melt in it all the time in order for the induction loop to work. Some foundries use both coreless and channel induction furnaces: a coreless furnace is used to melt the charge material, which is then transferred to the larger channel furnace for holding. Tapping the iron from the holding furnace reduces compositional variations, as each melted batch is mixed with previous batches. The composition of the melt can also be corrected in the holding furnace. [16]

A typical raw material batch for ductile iron consists of pig iron, low alloy steel scrap and foundry returns [16]. Different alloying materials are added during or after melting in order to obtain the desired carbon and silicon contents in the melt. Common materials used for increasing carbon or silicon content of the melt include different cokes (for increasing carbon content), FeSi (for increasing silicon content) and SiC (for increasing both carbon and silicon content) [23]. The chemical composition of the raw materials needs to be accurately known, as even small amounts of certain trace elements (discussed in Section 2.1.3) can negatively affect the shape on graphite nodules. This is especially true for SSF grade ductile irons, as they are also susceptible to elements that promote pearlite formation. Foundries that produce both conventional and SSF grade ductile irons face the practical problem that the foundry returns from these castings need to be separated. Otherwise returns containing high amounts of silicon might be used in production of conventional ductile iron grades, leading to failed melt batches.

2.3.2 Nodularization

Nodularizing elements need to be added to cast iron melt in order to produce spheroidal graphite. There are several elements that have this nodularizing effect (cerium, lithium, etc.), but magnesium is the industry standard used for nodularization treatment in cast irons. As mentioned in Section 2.1.3, magnesium reacts with sulfur, so the melt needs to have sufficiently low sulfur content before nodularization treatment in order to minimize the required magnesium addition. Figure 2.15 shows the relation between base iron sulfur content and magnesium addition: high base iron sulfur content requires higher magnesium additions to ensure nodular graphite shape. Magnesium starts to fade as soon as it is added to the molten iron, so the time between nodularization (and other melt treatments) and pouring should

be minimized. Magnesium content in ductile iron castings varies between 0.03 - 0.06 wt%, depending on the section thickness of the casting and the grade of ductile iron being produced, generally castings that cool faster require less magnesium. Too low magnesium levels lead to incomplete nodularization, which has a detrimental effect on mechanical properties of ductile iron, especially elongation. Adding too much magnesium is uneconomical and it can also cause carbide formation and shrinkage. [10, 16]

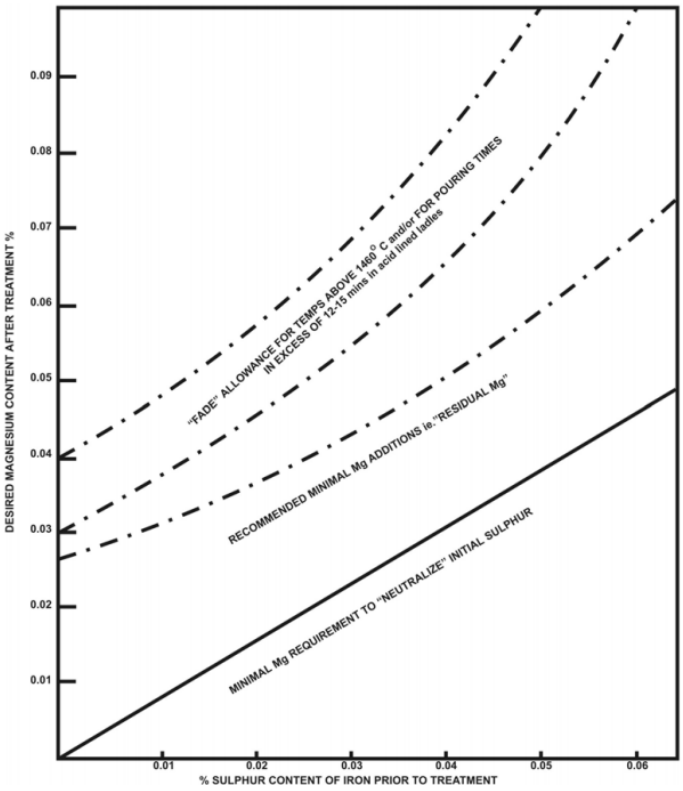

Figure 2.15 *Required magnesium addition based on base melt sulfur content in ductile iron production [9].*

Magnesium has low density, it is very reactive and it vaporizes at relatively low (about 1100 ℃) temperatures compared to cast iron melt treatment temperatures (about 1450 ℃). So if pure magnesium were added to molten cast iron, it would just burn away with no metallurgical effect. There are several common magnesium treatment methods. Usually magnesium is added as an alloy, which decreases magnesium reactivity. Sandwich method is a common and relatively simple method for magnesium treatment: FeSiMg alloy (containing 5-10 % Mg, reducing reactivity compared to pure Mg) is put on a pocket at the bottom of a treatment ladle and

covered with steel scrap to further slow vaporization of the magnesium. In addition, there are several commercial cover materials that slow down the vaporization and also act as inoculants. When the treatment ladle is filled with molten iron, the magnesium alloy at the bottom of the ladle vaporizes and reacts with the melt. Tundish cover process is a modification of the sandwich method: a cover is placed on top of the treatment ladle to reduce fume emissions and to improve magnesium yield. Sandwich and tundish cover magnesium treatment methods are illustrated in Figure 2.16. [10, 16]

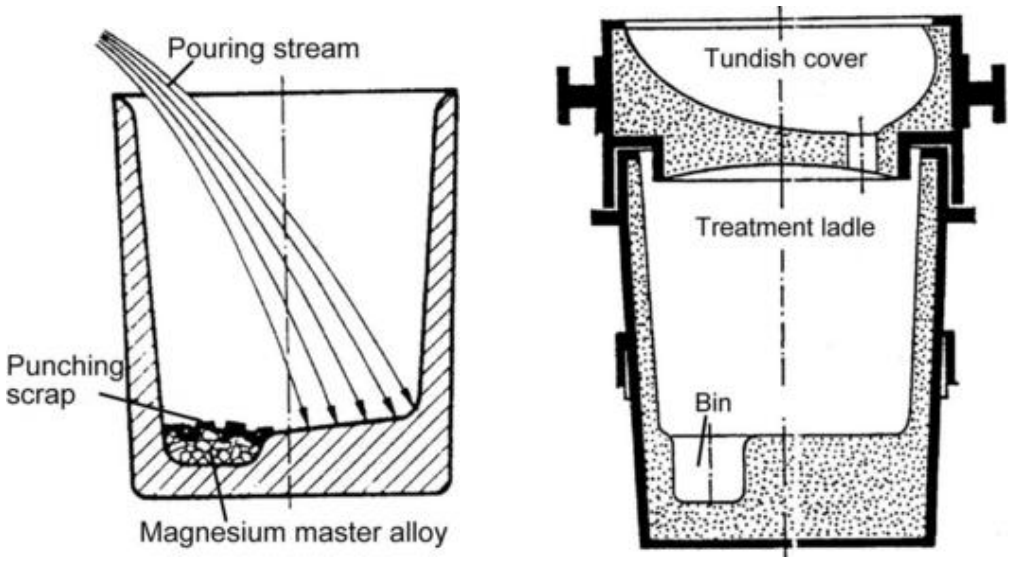

(a) Sandwich method. (b) Tundish cover method.

Figure 2.16 *Illustrations of common magnesium treatment methods [13].*

2.3.3 Inoculation

Inoculation is an important treatment for ductile irons as it creates sites for graphite nucleation. This increases nodule count, reduces undercooling and is important in order to avoid white solidification, which would reduce ductility. FeSi alloys (about 75 wt% Si) are commonly used for inoculation, they also include small amounts other elements (eg. barium, calcium) that increase the inoculation effect. There are several process points where the inoculation can be done: the inoculant can be added with nodulants at the bottom of the treatment ladle, they can be added to the melt stream or bottom of the casting ladle when the melt is poured from the

treatment ladle to the pouring ladle or they can be added to the melt stream or mold cavity during casting. The first three methods are called ladle inoculation and the latter two are known as late inoculation. The inoculation effect starts to fade as soon as the inoculants are added, so usually both ladle and late inoculation are used. [10, 16]

2.4 Cooling curve analysis of cast iron

Cooling curve analysis (CCA) is common tool in cast iron foundries, used to predict quality of the cast iron melt before casting. For example, CCA can be used determine the degree of inoculation, graphite morphology and shrinkage tendency of the melt [34]. Sand cups with disposable thermocouples are commonly used for CCA, as they are easy to use and require very little preparation. A sample cup with disposable thermocouple is shown in Figure 2.17. It should be noted that the cooling curve of the sample cup is different from that of the actual casting, as the cup is usually much smaller than actual castings and the sample cools below solidus temperature in under five minutes. So a CCA indicating good melt properties is not a guarantee of a successful casting.

Figure 2.17 *Cross-section of a disposable CCA sample cup [34].*

A cooling curve is simply the temperature measured from the sample as a function of time. An example of the cooling curve of a hypoeutectic cast iron is shown in Figure 2.18. The figure shows both the actual and theoretical cooling curve. The theoretical cooling curve assumes equilibrium state during eutectic solidification. However, cast iron solidification is a non-equilibrium process, so the actual cooling curve will differ from the theoretical one. The most obvious difference is the undercooling compared to eutectic temperature and subsequent increase in temperature due to heat generated by eutectic freezing [18]. Cooling curve analyses can also show the

first time derivative of temperature, cooling rate, as some changes are easier to see from the cooling rate curve than from the temperature curve. [34]

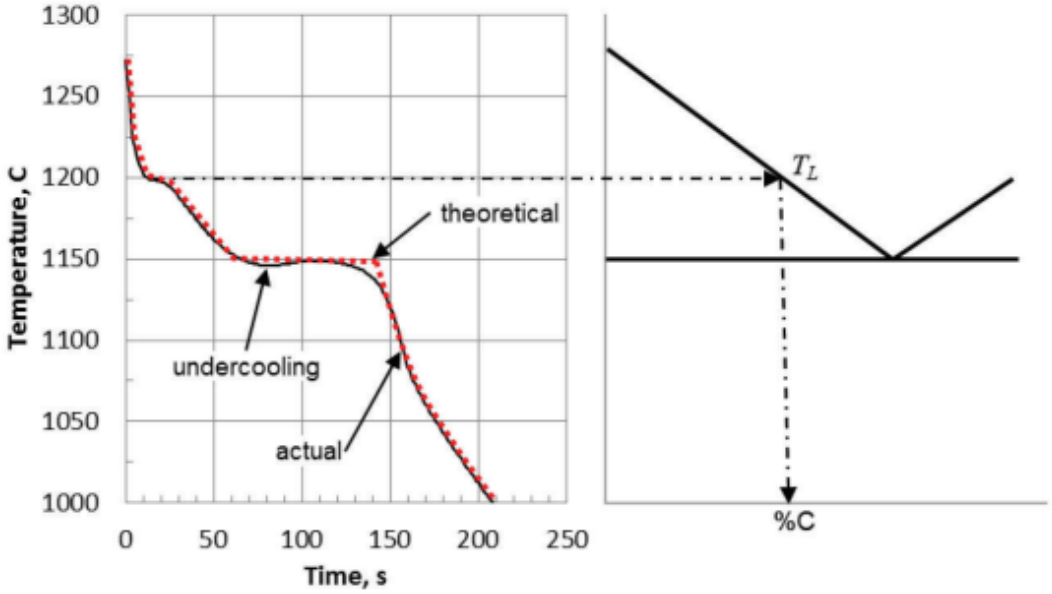

Figure 2.18 *Cooling curve of hypoeutectic cast iron [34].*

A ductile iron cooling curve is shown in Figure 2.19. Liquidus temperature (LT) is the start of dendritic solidification and it is the first arrest point in both curves. Even with eutectic melt composition, the melt can undercool below LT. The second arrest point is called low eutectic temperature (LET) and it is where the normal cooling is balanced by heat generated from eutectic solidification. This heat generation by graphite precipitation is powerful enough to actually cause the melt to warm up by several degrees, until the eutectic heat generation starts to fade and the curve reaches the third arrest point, high eutectic temperature (HET). Eutectic solidification and heat generation continue after HET, but they eventually fade as the whole melt has solidified and solidus temperature (ST) is reached. Recalescence (R) is another important parameter in CCA. It is the temperature difference between LET and HET. High R value (above 8 ℃) is an indication of high shrinkage potential and there are studies that show that high R values also correlate with CHG formation [33]. [18]

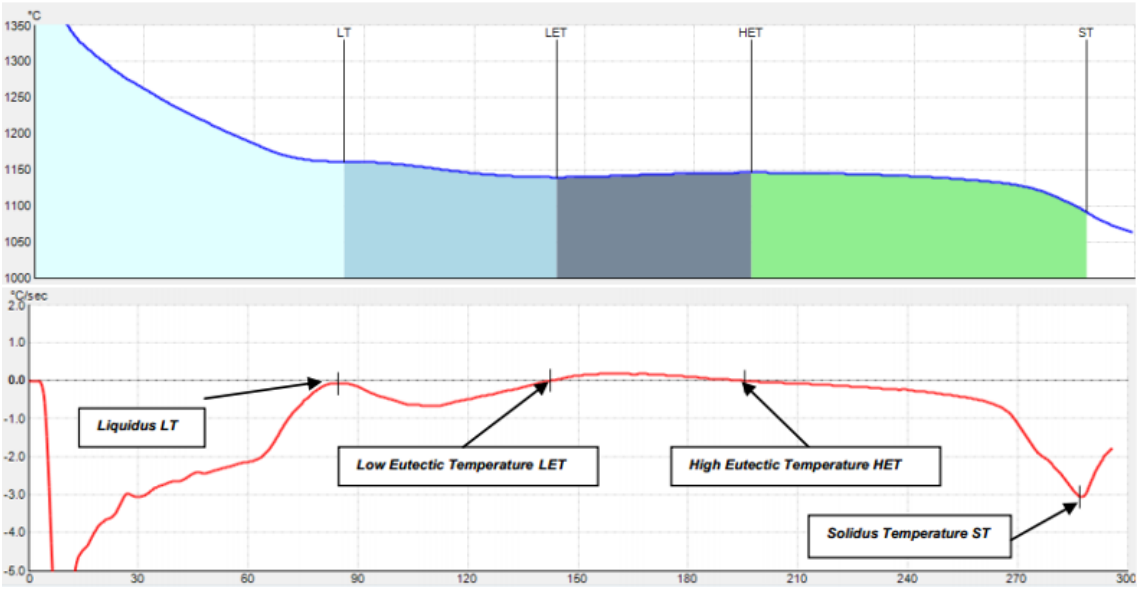

Figure 2.19 *Example cooling curve showing different arrest points. Adapted from [18]*

2.5 Solidification simulation of cast iron

There are two main simulation types used in cast iron production: solidification and filling simulation. Solidification simulations only simulate the solidification of an already full mold cavity (and attached feeders) where as a filling simulation simulates both the filling of the complete sand mold and its solidification (which usually starts before the whole mold has been filled). Filling simulations are obviously more complex and take longer to simulate, but they are typically done only just before production phase. Solidification simulations are relatively simple and fast to simulate and they are commonly used in product development phase. Solidification simulations are typically used to ensure the soundness of castings. If a simulation shows porosity in a critical area of a casting, the geometry of the casting can be changed or feeders or chills can be added to ensure directional solidification. Some advanced simulation software can also be used to predict other properties, such as microstructure or mechanical behavior of a casting.

There are several commercial casting simulation software available: CastCAE, MAGMA, NovaFlow/Solid and ProCAST, to name a few. Each simulation software uses some numerical simulation method for solving the fluid dynamic problems of mold solidification or filling. There are three main methods for solving these problems: finite difference method (FDM), finite volume method (FVM) and finite element method

(FEM) [10]. The simulation software used in this thesis uses the finite difference method [28]. A simplified explanation of this method is that it divides the fluid to non overlapping cuboid cells and calculates the fluid dynamic problems (e.g. heat flow) between the cells by solving a system of differential equations [21]. The benefit of this cuboid mesh is that it is relatively simple computationally [10]. However, representing more complex shapes such as curves with cuboids results in some inaccuracies. This can be countered by making the mesh finer, which then increases the time to complete the simulation. In addition to the mathematical model used by the software, the input data given by the user (pouring temperature, chemical composition, success of inoculation, etc.) significantly affects the accuracy of the simulation.

3. RESEARCH METHODS

The main objective of this thesis was to gain more insights on the production of GJS 600–10 grade SSF ductile iron. Separately cast tensile test bars were made to see how different nodulant and inoculant materials affect their mechanical properties. Cooling curve analysis was another important aspect of this thesis. Cooling curve samples were taken at different parts of the process to see how well cooling curve analysis predicts the properties of castings and tensile test bars.

Another aim of this thesis was to simulate solidification of tensile test specimens. SSF ductile iron grades from EN 1563 are relatively new, so it would be useful to know how well the simulation tools predict mechanical properties of tensile specimens and actual cast iron components made from SSF ductile iron. This would be a valuable tool for foundries, as quality assurance for mechanical properties of cast iron components is done by standardized tensile tests.

3.1 600-10 production trials

One batch of 600–10 melt was made for the production trial 1 and separately cast tensile test bars (called set A from now on) were produced. The diameter of the separately cast tensile test bar was about 28 mm (shown in Figure 3.3). The magnesium treatment was done with a FeSiMg alloy that contained minimal amounts of rare earth elements. The melt was inoculated twice, with ladle inoculant (also used as cover material for the FeSiMg alloy) and in-mold inoculant. The ladle inoculant was a FeSi based alloy with about 9 % barium and the late inoculant was also a FeSi based alloy containing about 1 % barium. A small amount of antimony was also added to the melt to prevent CHG formation.

Separately cast tensile test bars were also produced during production trial 2. Two sets of tensile test bars were cast, both were made from the same base melt and with the same FeSiMg alloy (same as in production trial 1) and same ladle inoculant , a

FeSi based alloy containing about 2 % barium (also used as cover material, different from the one used in trial 1). The addition of FeSiMg alloy was reduced based on the high residual magnesium levels in the first trial. The first set (set B) used a FeSi based alloy containing barium (same as the one used in trial 1) for mold inoculation and the second set (set C) used a FeSi based alloy containing about 4 % aluminum. Like in the first trial, a small amount of antimony was added to the melt in the second trial.

All of the bars were tested with standardized tensile test according to EN 6892 [3] and with Brinell hardness test according to EN 6506 [2]. The bars were also studied with optical microscope in order to observe the matrix and graphite morphologies. The nodularities of the micrographs were studied with a image analysis software called ImageJ. The nodularity values in this thesis are given as nodularity by count, which is calculated as the ratio between good nodules and all nodules in a micrograph, as shown in Equation 3.1. The limit value of circularity for a good nodule was 60 %.

$$\text{Nodularity} = \frac{\text{Good nodules}}{\text{All nodules}} \tag{3.1}$$

3.2 Thermal analysis of 600–10

This section introduces the cooling curve analysis equipment and parameters used in this thesis.

3.2.1 EPIC cooling curve analysis parameters

The cooling curve analyses for this thesis were made with EPIC thermal analysis system made by Elkem. The system consists of disposable sand cups with type K thermocouples connected to a data logger and a computer to save the data. The equipment is shown in Figure 3.1. EPIC can be used to monitor a wide variety of properties from the cast iron sample, this section will introduce those that important for this thesis and their effect on the solidification of cast iron. EPIC draws two curves from the cooling of the cast iron sample: cooling curve (temperature as a function of time) and cooling rate curve (first time derivative of temperature as a function of time). [18]

Figure 3.1 *EPIC thermal analysis equipment: sample cups, cup stand and data logger. [18]*

EPIC divides freezing to three stages: time between LT and LET, time between LET and HET and finally time between HET and ST. These stages are called G1, G2 and G3, respectively. G1 indicates dendritic freezing of austenite, G2 is the time between the start of eutectic precipitation and the peak graphite precipitation, and G3 is the late stage graphite precipitation that continues until ST. Steady late stage graphite precipitation minimizes shrinkage potential, so G3 should be maximized in ductile iron production. With properly inoculated ductile iron, there might be no undercooling after LT, so LT and LET might be the same temperature and G1 area is eliminated. Time between the start of eutectic precipitation and solidus (LET–ST) is another measure for good ductile iron melt, as it tells the total graphite precipitation time. As with G3, LET–ST should also be maximized in ductile iron production as it indicates well nucleated melt with reduced shrinkage tendency. [18]

Figure 3.2 shows a cooling curve taken from a conventional ductile iron melt during normal foundry operation. The sample was taken after magnesium treatment, ladle inoculation and slag removal, just before pouring. This cooling curve shows successful magnesium treatment and ladle inoculation. Graphite precipitation starts at LT, so there is no G1 stage. R value is low, so the G2 stage is very short. So most of the graphite precipitation happens during G3 stage, which results in steady and sustained graphite growth until very late stages of solidification. The cooling rate

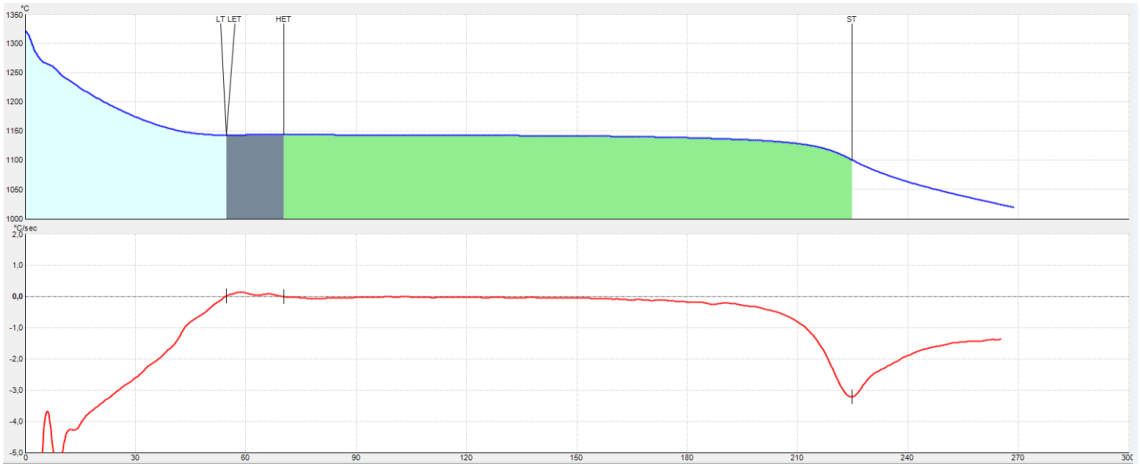

Figure 3.2 *Reference CCA of conventional ductile iron taken from normal foundry production after magnesium treatment and ladle inoculation.*

curve stays at or very near zero for most of the eutectic solidification phase and this long "eutectic plateau" is an indication of low shrinkage potential [18]. Table 3.1 shows reference values for conventional ductile iron CCA. It is not know that how well these correspond with CCA taken from SSF grade ductile irons.

Table 3.1 *Reference values for successful ductile iron CCA taken after magnesium treatment and inoculation. Adapted from [18].*

Parameter	Value	Explanation
LET	1140 or higher	Indication of nucleation potential.
R	As low as possible	Measure of undercooling and carbide potential.
G1	1% max.	Early stage graphite precipitation increases shrinkage.
G3	70 % or above	Late stage graphite precipitation counters shrinkage.
LET-ST	100 s or longer	Indicates controlled graphite growth.

3.2.2 Cooling curve analysis of production trials

Four cooling curve samples were taken during production trial 1. The samples were taken after slag removal and before pouring, like the reference cooling curve in Figure 3.2. The aim of these CCA tests was to determine if the base melt preparation and melt treatments were successful. It should be noted that these castings were

also post inoculated by mold inoculant and the effect of this final inoculation is not shown on the cooling curves.

Two cooling curve samples were taken from the second production trial, one from each set of tensile test bars. Like in the first trial, these samples were taken after slag removal, so they do not show the effect of late inoculation.

3.3 Solidification simulation of 600-10

This section introduces the simulation software and the parameters that are important for this thesis.

3.3.1 MAGMA simulation parameters

The solidification simulations for this thesis were done with MAGMA[5] simulation software from MAGMA Gießereitechnologie GmbH. MAGMA can be used to simulate solidification wide variety of different metals and alloys and it has a specific module for simulating cast iron. MAGMA is an advanced cast iron simulation tool, as it can predict the microstructure and mechanical properties of cast iron castings, in addition to mold filling and the formation of porosities during solidification. This section will introduce the MAGMA parameters important for this thesis.

Simulation of mechanical properties of cast iron is complex as it involves several simultaneous phenomena, including fluid flow, heat flow, diffusion, solidification and effect of inoculation. MAGMA takes numerous types of input data for simulations: heat flow, melt composition, type of mold and core sand, inoculation method etc. [28]. The parameters that were changed and tested in thesis were chemical composition of the melt and the type and amount of inoculation used. MAGMA divides inoculation method to three different parameters, these are shown in Table 3.2.

Table 3.2 *Melt treatment parameters for MAGMA[5] [28].*

Parameter	Options	Explanation
Inoculation method	poor, good, very good	Ladle inoculation, in-stream inoculation and combined ladle and in-stream inoculation, respectively.
Treatment yield	1 – 500 %	Used to modify the Inoculation method parameter. Values above 100 % indicate above normal inoculation yield.
Graptite precipitation	1 – 10	Parameter for graphite expansion potential: 10 means high potential and thus low shrinkage.

3.3.2 Solidification simulations of 600-10 tensile test bar

The solidification of a separately cast tensile test sample was simulated to see how well the simulated mechanical properties correspond with the actual mechanical properties of the tensile specimens cast during production trial 1. The 3D CAD model used for these simulations is shown in Figure 3.3. The chemical composition used for the simulations was sample 1 taken from analysis of the actual 600–10 castings from production trial 1, shown in Table 4.2. The simulation used the complete chemical analysis, so several other elements are considered in addition to those shown in Table 4.2. The chemical composition of 600–10 grade is a complication for these simulations, as 600–10 grades usually contain up to 4.3 wt% of silicon [1], but the manual for MAGMA recommends that 4.0 wt% is the maximum silicon content used for simulations [28]. Three simulation versions were made, each with different inoculation parameters. The different versions simulated normal, excellent and slightly failed inoculation, respectively. The simulation parameters are shown in Table 3.3.

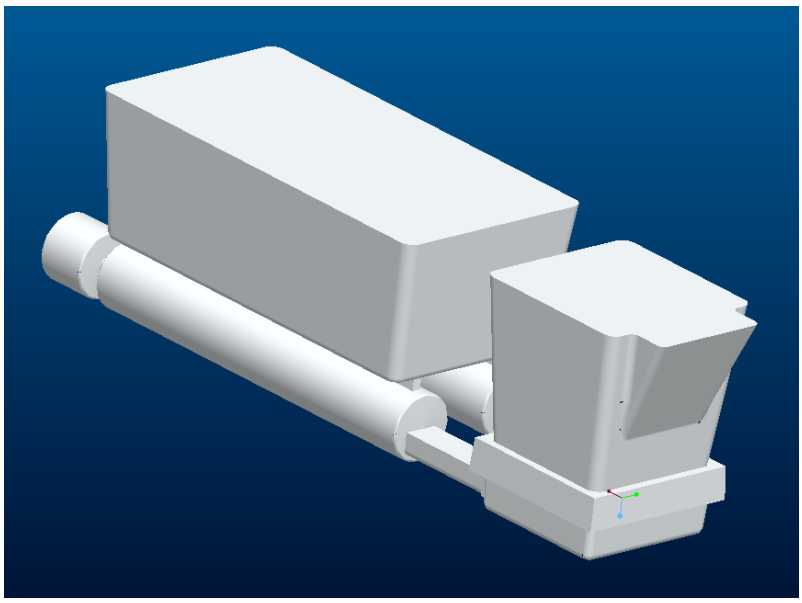

Figure 3.3 *3D CAD model of separately cast tensile test sample*

Table 3.3 *Melt treatment parameters used for solidification simulations*

Version	Success of inoculation	Inoculation method	Treatment yield	Graphite precipitation
v01	Normal (good)	Good	100	8
v02	Excellent	Very good	100	10
v03	Fair	Good	80	6

4. RESULTS

This chapter presents the results of the production trials, the related cooling curve analyses and finally the solidification simulation tests. In addition to the mechanical tests, chemical analyses and micrographs were taken from the samples to understand the cause of the mechanical behavior.

4.1 Mechanical properties, micrographs and chemical analyses

The tensile and hardness test results from production trial 1 are shown in Table 4.1 and Figure 4.1 shows micrographs of the separately cast tensile test bars. Table 4.2 shows chemical analyses taken from the molds during the production trial. Each sample corresponds with a different treatment and casting ladle.

Table 4.1 *Tensile and hardness trial results from production test 1.*

Sample	Yield strength [MPa]	Tensile strength [MPa]	Elongation [%]	Hardness [HB]
A1	519	624	14.0	207
A2	530	630	14.6	212
A3	526	636	15.8	217
A4	526	637	14.8	217

Table 4.2 *Chemical analyses taken from castings during production trial 1.*

Sample	C [wt%]	Si [wt%]	S [wt%]	Mg [wt%]	CE
A1	2.86	4.25	0.010	0.059	4.29
A2	2.83	4.35	0.010	0.065	4.30
A3	2.86	4.31	0.010	0.061	4.31
A4	2.91	4.19	0.012	0.061	4.32

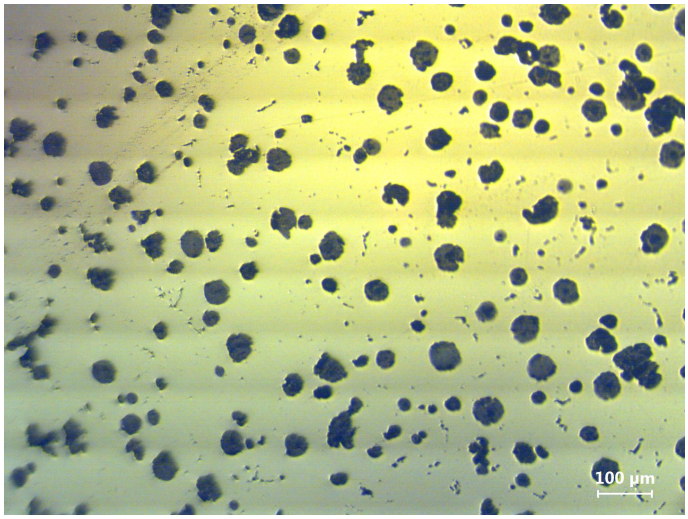

(a) Sample A2. Nodularity 83 %.

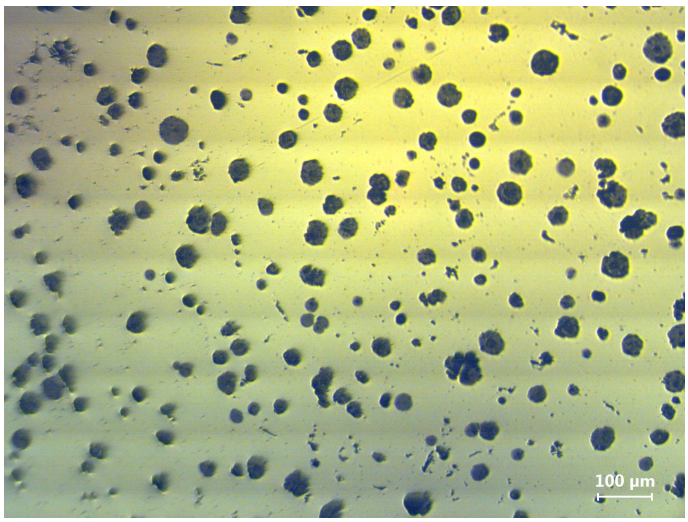

(b) Sample A4. Nodularity 80 %.

Figure 4.1 *Micrographs of separately cast tensile test bars made in production trial 1. Both unetched.*

Table 4.3 shows tensile and hardness test results from production trial 2 and Figure 4.2 shows micrographs taken from the tensile test bars. Table 4.4 shows chemical analyses taken from the tensile test bars.

Table 4.3 *Tensile and hardness test results from production trial 2.*

Sample	Yield strength [MPa]	Tensile strength [MPa]	Elongation [%]	Hardness [HB]
B1	485	574	11.4	201
B2	480	576	12.1	212
C1	492	592	13.9	207
C2	500	595	14.3	207

Table 4.4 *Chemical analyses taken from tensile test bars during production trial 2.*

Sample	C [wt%]	Si [wt%]	S [wt%]	Mg [wt%]	CE
B	3.05	4.24	0.008	0.041	4.46
C	3.05	4.24	0.008	0.041	4.46

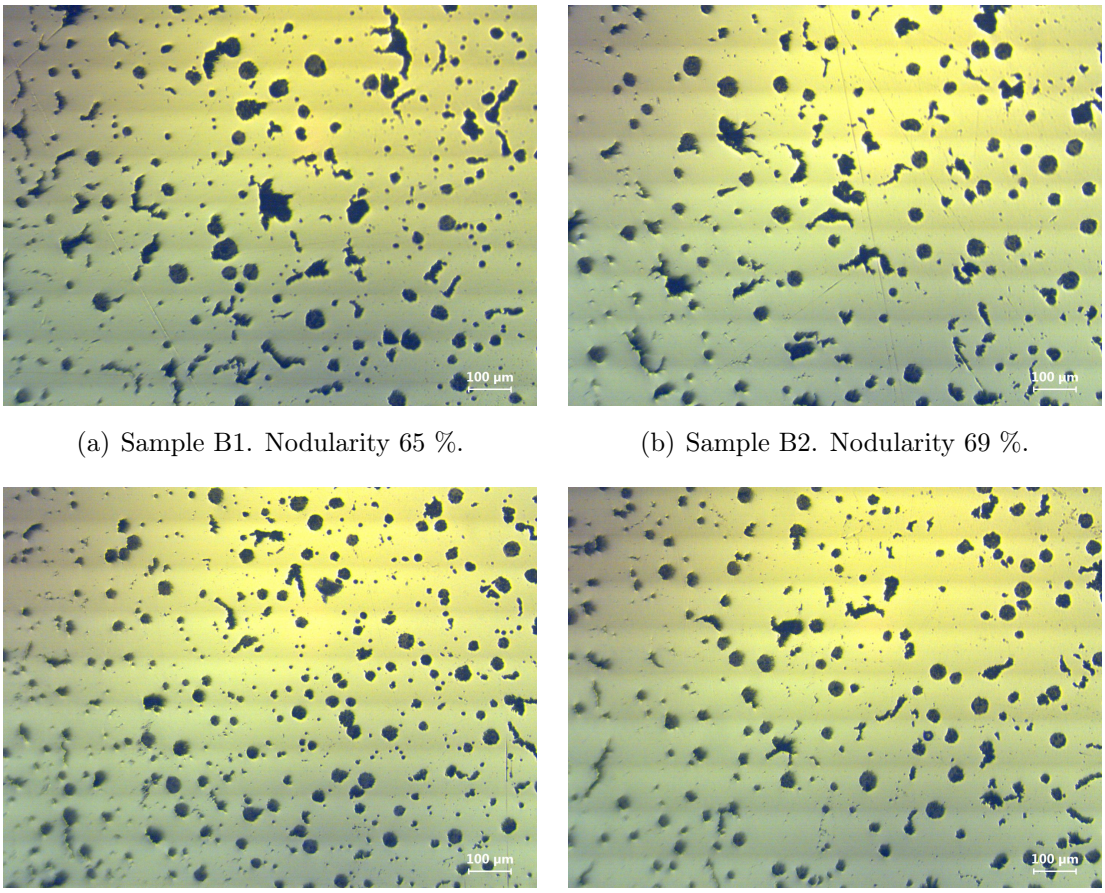

(a) Sample B1. Nodularity 65 %.

(b) Sample B2. Nodularity 69 %.

(c) Sample C1. Nodularity 78 %.

(d) Sample C2. Nodularity 72 %.

Figure 4.2 *Micrographs of separately cast tensile test bars made in production trial 2. All unetched.*

4.2 Cooling curves of SSF production trials

The cooling curves taken during production trial 1 are shown in Figure 4.3. The CCA results from these samples are shown in Table 4.5, which also shows the average and standard deviation of the values.

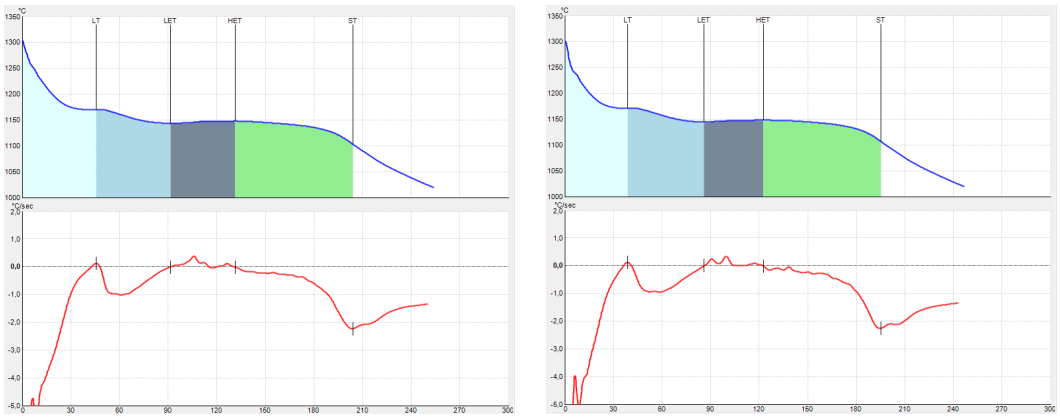

(a) Sample A1 (b) Sample A2

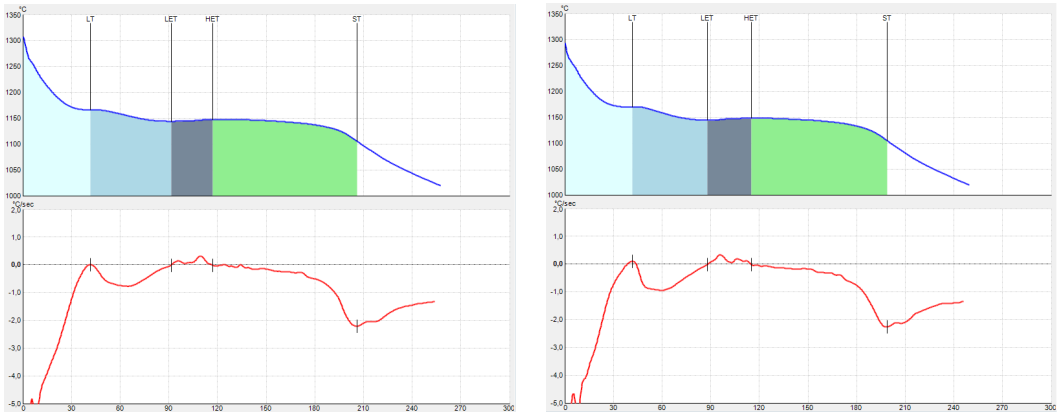

(c) Sample A3 (d) Sample A4

Figure 4.3 *Cooling curves from production trial 1.*

Table 4.5 *CCA results of production trial 1.*

Sample	LT [°C]	LET [°C]	LET-ST [s]	R [°C]	G1 [%]	G2 [%]	G3 [%]
A1	1170	1144	112.5	4.1	29	25	46
A2	1171	1145	109.2	3.8	30	23	47
A3	1166	1144	114.6	3.4	31	16	53
A4	1170	1145	110.7	4.2	30	17	53
Avg	1169	1145	111.8	3.9	30	20	50
SD	2.2	0.6	2.3	0.4	0.8	4.4	3.8

Cooling curves were taken during production in production trial 2 and they are shown in Figure 4.4 and the CCA results in Table 4.6.

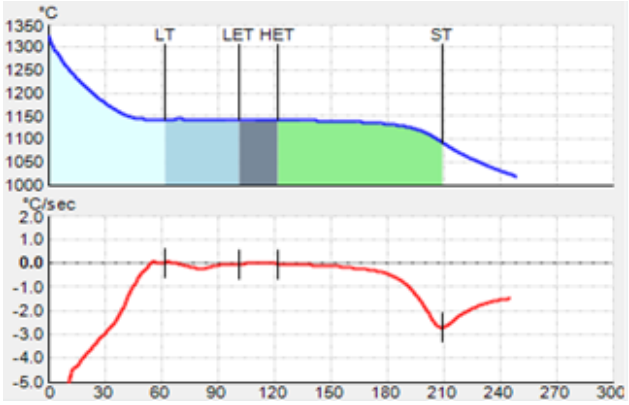

(a) Sample B

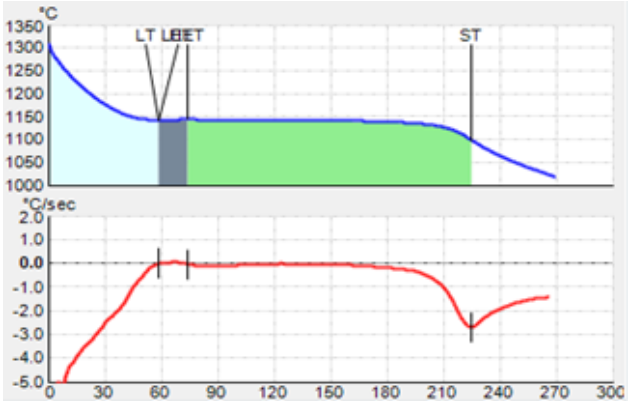

(b) Sample C

Figure 4.4 *Cooling curves from production trial 2.*

Table 4.6 *CCA results of production trial 2.*

Sample	LT [°C]	LET [°C]	LET-ST [s]	R [°C]	G1 [%]	G2 [%]	G3 [%]
B	1144	1142	108.3	0.3	27	14	59
C	1144	1144	166.7	0.8	1	9	90

4.3 Simulated mechanical properties of tensile test bar

Table 4.7 shows the results of the tensile test bar solidification simulations. MAGMA gives the three different results for strength and elongation values and these are listed in the following order: minimum, mean and maximum. Table 4.8 shows the microstructure of the tensile test bar given by the solidification simulation.

Table 4.7 *Mechanical properties of tensile test bar solidification simulations. Minimum, mean and maximum values, respectively.*

Simulation version	Yield strength [MPa]	Tensile strength [MPa]	Elongation [%]	Hardness [HB]
v01	370 - 425 - 480	585 - 665 - 735	4 - 8 - 12	220
v02	360 - 420 - 470	570 - 650 - 720	4 - 9 - 13	215
v03	370 - 430 - 485	590 - 670 - 740	4 - 8 - 11	225

Table 4.8 *Microstructure of tensile test bar solidification simulations.*

Simulation version	Fraction of ferrite [%]	Fraction of pearlite [%]
v01	95	5
v02	99	0
v03	93	6

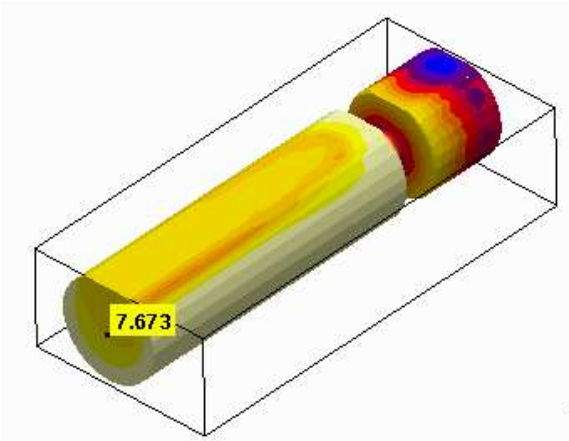

Figure 4.5 *Point used for simulation results.*

All of the values given in the previous two tables were taken from a point in the center of the tensile test bar, which corresponds with the area where a real tensile test specimen would fracture. The location of this point is shown in Figure 4.5. The mechanical properties are not homogeneous throughout the bar. The variation of mechanical properties is shown in Figure 4.6. This figure shows the variation of mean tensile strength and mean elongation, but the variation was similar with other properties as well.

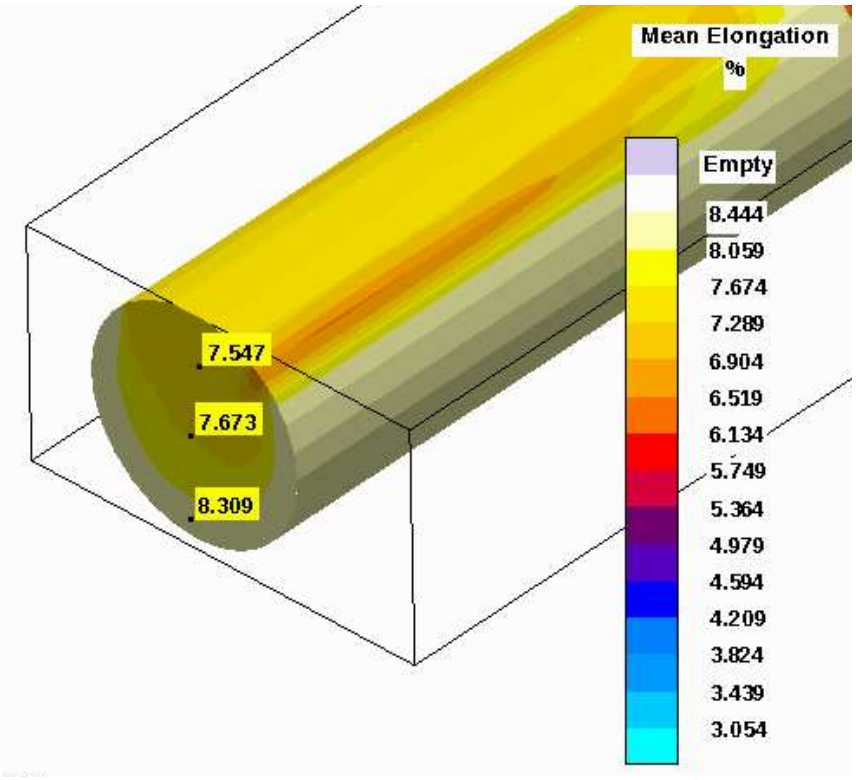

(a) Mean elongation

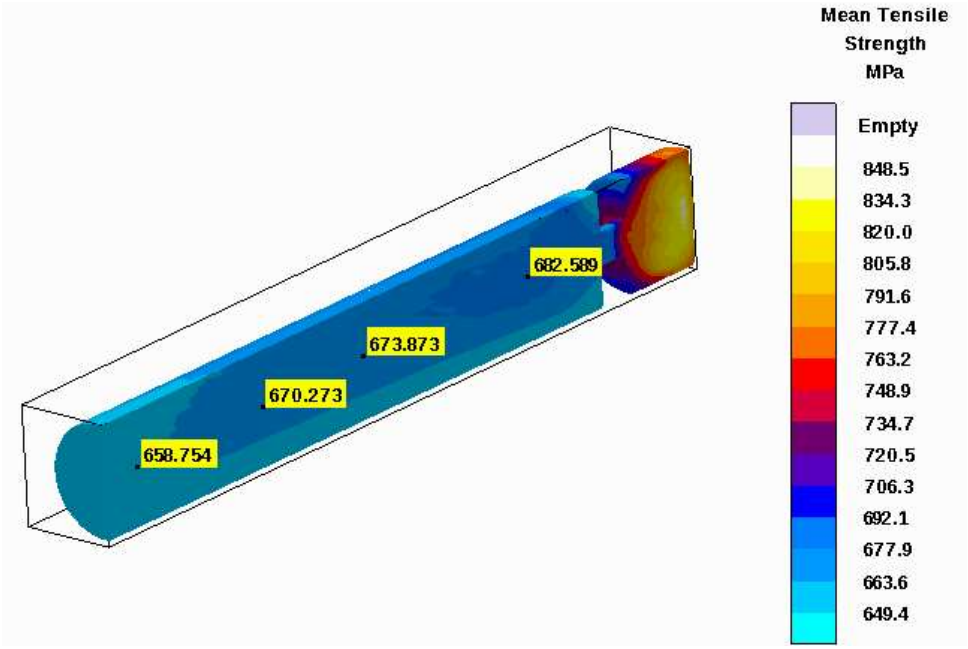

(b) Mean tensile strength

Figure 4.6 *Variation of simulated mechanical properties. Taken from simulation v03.*

5. DISCUSSION

This chapter discusses the results of the production trials and how the cooling curve analyses can predict the mechanical properties and microstructure of the tensile test bars. The results of the solidification simulation are analyzed to see if it can used as a tool for designing castings made of SSF ductile iron grades.

5.1 Mechanical properties and microstructure

The mechanical properties of the separately cast tensile bars of production trial 1 (Table 4.1) were excellent, with tensile strength values of about 630 MPa and elongation values of over 14 %, which are both well above the standard requirements for 600–10 grade. The microstructure of these samples, shown in Figure 4.1, contains some imperfect nodules and the samples have nodularity of about 80 %. This quite clearly shows that these SSF grade ductile irons can have sufficient mechanical properties even with only 80 % nodularity, at least for static loading conditions. The samples contained high levels of residual magnesium (0.059 wt% and above), so the addition of FeSiMg alloy was lowered for production trial 2.

The separately cast tensile test bars from the second production trial show mechanical properties slightly below standard requirements, with tensile strength values of about 575 MPa for the B bars and 595 MPa for C bars. Both sets were made from the same base melt and they underwent nodularization and ladle inoculation in the same ladle, so the only difference is the late inoculant material. The late inoculant used for C bars provided slightly better results. The silicon content of these bars (shown in Table 4.4) were comparable to the ones in the first production trial, so the solid strengthening effect of silicon should be present. The micrographs of these test bars (Figure 4.2) show poor nodularity, 65 – 69 % for B bars and 72 – 78 % for C bars. Some of the graphite has precipitated as compacted graphite (form III of EN 945, Figure 2.4), especially in the B bars. The chemical analyses show much lower magnesium content (0.041 wt%) than in the first trial, which suggests that

the FeSiMg alloy addition was lowered too much. There was not enough magnesium to form nodules of all of the graphite. More powerful inoculants might have also improved the mechanical properties of these tensile test bars.

5.2 Cooling curve analysis

The cooling curves for production trial 1 were taken after magnesium treatment and ladle inoculation, but before late inoculation. These curves (shown in Figure 4.3) show poor inoculation, as they have high G1 phase and average G3 phase of only 50 %. LET-ST values have an average of 112 s, which might cause imperfect graphite nodules. Castings made from this melt (without late inoculation) would probably show worse mechanical properties and high shrinkage in castings. However, the separately cast tensile test bars made from this melt showed excellent mechanical properties, so the late inoculant material seems to be potent enough for 600–10 grade SSF irons.

The cooling curve samples in production trial 2 were taken after late inoculation, with B and C samples having different late inoculant material. The cooling curve (shown in Figure 4.4) for sample B is quite similar with the curves from production trial 1, with significant G1 area (27 %) and LET-ST of only 108 s. Sample C seems to be excellent from the point of cooling curve analysis, with no G1 area, long and steady graphite precipitation and LET-ST of 167 s. However, the mechanical properties of these tensile test bars do not meet the standard requirements. Sample B shows higher G2 values than sample C (14 and 9 %, respectively) and compacted graphite is formed in the G2 area [18]. This corresponds with the microstructure of the test bars (Figure 4.2), with sample B showing more compacted graphite and poorer nodularity. The cooling characteristics of the cooling curve sample and a separately cast tensile test bar are different, so the mechanical properties of a tensile test bar or casting cannot be predicted solely from a cooling curve sample.

5.3 Solidification simulation

Out of the three different simulation versions, only the one with the highest inoculation yield (v02) has completely ferritic matrix structure (Table 4.8). The other two show small amounts of pearlite formation. Simulation v02 has the lowest strength (both tensile and yield) and hardness values of the three tests (Table 4.7). The

software gives three different values for strength and elongation and for version v02 the ones closest to the actual values (separately cast samples, Table 4.1) were maximum yield strength, mean tensile strength and maximum elongation (470 MPa, 650 MPa and 13 %, respectively). The average errors were 55 MPa (11 %) for yield strength, 18 MPa (3 %) for tensile strength and 1.5 % (12 %) for elongation. These results are collected in Table 5.1. These simulated results are quite close to the actual tensile test bar mechanical properties.

Table 5.1 *Comparison of mechanical properties between actual and simulated tensile test bars.*

	Yield strength [MPa]	Tensile strength [MPa]	Elongation
Test bars (average)	525	632	14.8
Simulated (v02)	470	650	13
Absolute error	55	18	1.8
Relative error	0.11	0.03	0.12

It should be noted that the simulation gives too low yield strength and elongation values and too high tensile strength values. So MAGMA does not completely take into account of the solid solution strengthening effect of silicon, as ratio between simulated (maximum) yield and tensile strengths is about 65 %, which is normal for conventional ductile irons but should be higher for SSF grades. The simulations versions v01 and v03 with slightly pearlitic matrix structure are stronger than and harder than the completely ferritic v02. This suggest that the simulation does not completely understand the chemical composition and mechanical properties, but treats them as conventional cast irons with significant amounts of solid solution strengthening from silicon. The manual for MAGMA also suggested this, as it mentioned that maximum silicon content used for simulations should be 4.0 wt% [28].

5.4 Suggestions for further research

An obvious addition the cooling curve analyses done during production trial 1 would be to take some samples from the mold, so they would show the effect of late inoculation as well. It would also be useful to take samples at different times of the

process. For example, taking cooling curve samples from first and last mold poured from the same ladle would show whether the magnesium treatment and/or the ladle inoculation had started to fade. Taking samples from different melt treatment steps would show how each of them affects the cooling curve. So samples would need to be taken from the base melt, after nodularization/ladle inoculation and after late inoculation. This could be used to rank each treatment material and method and also their combinations.

6. SUMMARY

Production trial 1 was successful. The separately cast tensile test bars made of 600–10 SSF ductile iron showed excellent mechanical properties, significantly higher strength and elongation values than EN standard 1563 dictates. While the cooling curve analyses taken during the trial showed insufficient ladle inoculation, the late inoculant is potent enough to ensure good mechanical properties. Cooling curve analyses should be done at several points during the melt treatment process to see how each nodulant or inoculant material affects the cooling characteristics.

The melt treatment process was similar between the two different tensile test samples in production trial 2, with only the late inoculant material being different. Both sets of separately cast tensile test bars did not meet the mechanical properties of EN standard 1563. Micrographs taken from the test bars suggest that poor nodularization was the cause for poor mechanical properties. Changing the nodulant and inoculant materials for more potent ones might improve the mechanical properties, or simply adding more nodulant might have the same effect. The cooling curve analyses done in this trial show that the increased amount of compacted graphite formation is partly predicted by the cooling curve. But even good cooling curve does not ensure high strength and elongation properties, as cooling curve analysis is better suited for measuring shrinkage potential or formation of detrimental graphite forms in cast irons.

The solidification simulations show that the simulation software does not yet completely understand the properties of SSF ductile irons. But the simulations do predict mechanical properties of the same magnitude as the actual tensile test bars. So even though these simulations cannot be used to pinpoint the exact mechanical properties of an specific area in a casting, they can still be used locate thermal centers and possible weak spots in the castings.

The production of EN GJS 600–10 grade is more complex than production of conventional ductile irons or other SSF grade ductile irons. The chemical composition

of the raw materials needs to be known precisely, as even small quantities of several elements can be detrimental for the mechanical properties of the material and the silicon content of the material is at its limit. The cooling curve analyses done for this thesis showed that all of the melt treatment stages were not successful and some further studies are needed to find out which nodulant and inoculant materials are best suited for production of 600-100 grade ductile iron. But even now the EN GJS 600–10 grade shows great promise, as the tensile test results from the first production trial notably exceeded the standard requirements.

BIBLIOGRAPHY

[1] "EN ISO 1563, Founding - Spheroidal graphite cast irons," Finnish Standards Association, Helsinki, 2011, 46 p.

[2] "EN ISO 6506, Metallic materials – Brinell hardness test – Part 1: Test method," Finnish Standards Association, Helsinki, 2014, 16 p.

[3] "EN ISO 6892, Metallic materials – Tensile testing – Part 1: Method of test at room temperature ," Finnish Standards Association, Helsinki, 2009, 65 p.

[4] "EN ISO 945, Microstructure of cast irons - Part 1: Graphite classification by visual analysis," Finnish Standards Association, Helsinki, 2008, 19 p.

[5] *Metals Handbook Desk Edition.* ASM International, 1998, available (accessed 9.11.2015): http://products.asminternational.org/hbk/index.jsp.

[6] *Encyclopedia of Materials: Science and Technology.* Elsevier Ltd, 2001, pp. 1003-1011.

[7] *ASM Handbooks Online, Volume 9: Metallography and Microstructures.* ASM International, 2004, available (accessed on 1.3.2016): http://products.asminternational.org/hbk/index.jsp.

[8] "Graphite structures in cast irons," Elkem AS, 2004, Foundry datasheet.

[9] "Magnesium versus sulphur in ductile iron," Elkem AS, 2004, Foundry datasheet.

[10] *ASM Handbooks Online, Volume 15: Castings.* ASM International, 2008, available (accessed on 2.11.2015): http://products.asminternational.org/hbk/index.jsp.

[11] *ASM Handbooks Online, Volume 3: Alloy Phase Diagrams.* ASM International, 2012, available (accessed on 22.10.2015): http://products.asminternational.org/hbk/index.jsp.

[12] *ASM Handbooks Online, Volume 1: Properties and Selection: Irons, Steels, and High-Performance Alloys.* ASM International, 2014, available (accessed on 29.10.2015): http://products.asminternational.org/hbk/index.jsp.

[13] *ASM Handbooks Online, Volume 4C: Induction Heating and Heat Treatment.* ASM International, 2014, available (accessed on 20.3.2016): http://products.asminternational.org/hbk/index.jsp.

[14] A. Alhussein, M. Risbet, A. Bastien, J. Chobaut, D. Balloy, and J. Favergeon, "Influence of silicon and addition elements on the mechanical behavior of ferritic ductile cast iron," *Materials Science & Engineering A*, 2014.

[15] E. Autere, Y. Ingman, and P. Tennilä, *Valimotekniikka.* Insinööritieto Oy, 1986.

[16] J. R. Brown, *Foseco Ferrous Foundryman's Handbook.* Butterworth-Heinemann Ltd, 1999.

[17] W. D. Callister, *Materials Science and Engineering: An Introduction*, 7th ed. John Wiley & Sons, Inc., 2007.

[18] *EPIC^{TM} Thermal Analysis User Manual*, Elkem AS.

[19] P. Ferro, A. Fabrizi, R. Cervo, and C. Carollo, "Effect of inoculant containing rare earth metals and bismuth on microstructure and mechanical properties of heavy-section near-eutectic ductile iron castings," *Journal of Materials Processing Technology*, vol. 213, pp. 1601–1608, 2013.

[20] P. Ferro, P. Lazzarin, and F. Berto, "Fatigue properties of ductile cast iron containing chunky graphite," *Materials Science and Engineering A*, vol. 554, pp. 122–128, 2012.

[21] J. H. Ferziger and M. Peric, *Computational Methods for Fluid Dynamics*, 3rd ed. Springer-Verlag Berlin Heidelberg, 2002.

[22] G. M. Goodrich, Ed., *Iron Castings Engineering Handbook.* American Foundry Society, 2006.

[23] R. Keskinen and P. Niemi, "Valuraudan sulatus ja käsittely," Valuatlas learning material, available (accessed 6.4.2016): http://www.valuatlas.fi/tietomat/koosteet/sulatus_tao/index.html.

[24] R. Källbom, K. Hamberg, M.Wessén, and L.-E. Björkegren, "On the solidification sequence of ductile iron castings containing chunky graphite," *Materials Science and Engineering A*, vol. 413–414, pp. 346–351, 2006.

[25] C. Labreque and M. Gagne, "Ductile iron: Fifty years of continuous development," *Canadian Metallurgical Quarterly*, vol. 37, 1998.

[26] J. Lacaze, S. Armendariz, P. Larrañaga, I. Asenjo, J. Sertucha, and R. Suárez, "Effect of carbon equivalent on graphite formation in heavy-section ductile iron parts," *Materials Science Forum*, vol. 636–637, pp. 523–530, 2010.

[27] P. Larrañaga, I. Asenjo, J. Sertucha, R. Suarez, I. Ferrer, and J. Lacaze, "Effect of antimony and cerium on the formation of chunky graphite during solidification of heavy-section castings of near-eutectic spheroidal graphite irons," *Metallurgical and Materials Transactions A*, vol. 40, pp. 654–661, 2009.

[28] *MAGMA 5.0 User Manual*, MAGMA Gießereitechnologie GmbH.

[29] S. Meskanen and E. Niini, "Valuraudat," Valuatlas learning material, available (accessed 9.11.2015): http://www.valuatlas.fi/tietomat/koosteet/valimotekniikanperusteet/.

[30] H. Nakae, S. Jung, and H.-C. Shin, "Formation mechanism of chunky graphite and its preventive measures," *Journal of Materials Science and Technology*, vol. 24, pp. 289–295, 2008.

[31] F. B. Pickering, *Physical metallurgy and the design of steels.* Applied Science Publishers, 1978.

[32] S. Schmauder and C. Kohler, "Atomistic simulations of solid solution strengthening of α-iron," *Computational Materials Science*, vol. 50, no. 4, pp. 1238 – 1243, 2011.

[33] J. Sertucha, R. Suárez, I. Asenjo, P. Larrañaga, J. Lacaze, I. Ferrer, and S. Armendariz, "Thermal analysis of the formation of chunky graphite during solidification of heavy-section spheroidal graphite iron parts," *ISIJ International*, vol. 49, pp. 220–228, 2009.

[34] D. Stefanescu, "Thermal analysis – theory and applications in metalcasting," *International Journal of Metalcasting*, vol. 9, 2015.

[35] W. Stets, H. Löblich, G. Gassner, and P. Schumacher, "Solution strengthened ferritic ductile cast iron properties, production and application," *International Journal of Metalcasting*, vol. 8, 2014.